Extratropical Air-Sea Interaction, SST Variability and the Pacific Decadal Oscillation (PDO)

By Michael Alexander

Chapter 7 in the AGU Monograph
Climate Dynamics: Why Does Climate Vary?

Submitted September 2008
Revised June 2009

Michael Alexander
NOAA/Earth System Research Laboratory
R/PSD1
325 Broadway
Boulder, CO 80305-3328
USA
Michael.Alexander@noaa.gov

ABSTRACT

We examine processes that influence North Pacific sea surface temperture (SST) anomalies including surface heat fluxes, upper-ocean mixing, thermocline variability, ocean currents and tropical-extratropical interactions via the atmosphere and ocean. The ocean integrates rapidly varying atmospheric heat flux and wind forcing and thus a stochastic model of the climate system, where white noise forcing produces a red spectrum, appears to provide a baseline for SST variability even on decadal time scales. However, additional processes influence Pacific climate variability including the "reemergence mechanism" where seasonal variability in mixed layer depth allows surface temperature anomalies to be stored at depth during summer and return to the surface in the following winter. Wind stress curl anomalies in the central/east Pacific drive thermocline variability that propagates to the west Pacific, via baroclinic Rossby waves and influences SST by vertical mixing and the change in strength and position of the ocean gyres. Atmospheric changes associated with ENSO also influence North Pacific SST anomalies via the "atmospheric bridge".

The dominant pattern of North Pacific SST anomalies, the "Pacific Decadal Oscillation" (PDO), exhibits variability on interannual as well as decadal time scales. Unlike ENSO, the PDO does not appear to be a mode of the climate system but rather it results from several different mechanisms including *i)* stochastic heat flux forcing associated with random fluctuations in the Aleutian low, *ii*) the atmospheric bridge augmented by the reemergence mechanism and *iii)* wind-driven changes in the North Pacific gyres.

1) INTRODUCTION

There are several reasons why the oceans play a key role in climate variability at interannual and longer time scales. Due to the high specific heat and density of sea water, the heat capacity of an ocean column ~2.5 m deep is as large as the entire atmosphere above it. In addition, the upper ocean is generally well mixed and sea surface temperature anomalies (SSTAs) extend over the depth of the mixed layer tens to hundreds of meters below the surface. As a result SSTA, the primary means through which the ocean influences the atmosphere, can persist for months or even years. In addition to thermodynamic considerations, many dynamical ocean processes are much slower than their atmospheric counterparts. For example, relatively strong currents such as the Gulf Stream and Kuroshio are on the order of 1 m s^{-1} roughly two orders of magnitude slower than the jet stream in similar locations. Midlatitude ocean gyres take 5-10 years to fully adjust to the wind forcing that drives them and exchanges with the deeper oceans, via meridional overturning circulations, can take decades to centuries.

Beginning with the pioneering work of *Namias* [e.g. 1959, 1963, 1965, 1969] and *Bjerknes* [1964], many studies have sought to understand the temporal and spatial structure of midlatitude SSTAs and the extent to which they influence the atmosphere. The dominant pattern of SST variability over the North Pacific exhibited pronounced low-frequency fluctuations during the 20^{th} century and was thus termed the Pacific Decadal Oscillation (PDO) by *Mantua et al.* [1997]. The fluctuations in the PDO have been linked to many climatic and ecosystem changes and thus has become a focal point for studies of Pacific climate variability. In this chapter, we examine processes that

73 influence extratropical SST anomalies and mechanisms for generating Pacific decadal
74 variability including the PDO.

75 This chapter is structured as follows: basic properties of the North Pacific Ocean
76 including the mean SST and its interannual variability, the vertical structure of
77 temperature and the three-dimensional flow are described in section 2; the terms that
78 contribute to the surface heat budget and thus the SST tendency are examined in section
79 3; the processes that generate and maintain North Pacific SST anomalies, including
80 stochastic forcing, upper ocean mixing, ocean currents and Rossby waves, dynamic
81 extratropical air-sea interaction and teleconnections from the tropics are explored in
82 section 4. The PDO and its underlying causes are described in section 5, while section 6
83 examines other potential sources of variability and processes/patterns that occur in other
84 extratropical ocean basins.

85

86 2) MEAN UPPER OCEAN CLIMATE

87 North Pacific SST variability is strongly shaped by the climate and circulation of the
88 upper ocean. The mean SST field features nearly zonal isotherms across most of the
89 Pacific with a strong gradient near 40ºN, indicative of the subpolar front (consisting of
90 the Oyashio and Kuroshio fronts with a mixed water region in between) that separates the
91 two main gyres in the North Pacific (Figure 1a). In the eastern Pacific, the curvature of
92 the isotherms is consistent with the structure of the currents where the subpolar gyre turns
93 north and the subtropical gyre south (Figure 2). The weaker subtropical front, which is
94 more prominent in the SST standard deviation (σ) field (Figure 1b) than in the mean SST
95 field, extends southwestward from approximately 35°N, 135°W to 20°N, 180°. The mean

96 isotherms bulge north in the vicinity of Japan associated with the warm water transport
97 by the Kuroshio current, which turns eastward between 35°-40°N as the Kuroshio
98 Extension (KE) and then the North Pacific Current. SST variance maxima are located
99 along the KE/subpolar front, the subtropical front, in the Bering Sea and along the coast
100 of North America (Figure 1b).

101 The surface layer over most of the world's oceans is vertically well mixed and thus,
102 heating/cooling from the atmosphere spreads from the surface down to the base of the
103 mixed layer (h). Due to the large thermal inertia of the surface layer, SSTs reach a
104 maximum in August-September and a minimum in March (Fig. 3), about three months
105 after the respective maximum and minimum in solar forcing, compared to a one month
106 lag for land temperatures. Beneath the warm shallow mixed layer in summer lies the
107 seasonal thermocline where the temperature rapidly decreases with depth. The mixed
108 layer is deepest in late winter, when it ranges from 100 m over much of the North Pacific
109 and 200 m in the KE region but shoals to around 20-30 m in late spring and summer
110 (Figures 3 and 4). Since h is approximately 5–20 times smaller in summer than in winter,
111 less energy is required to heat/cool the mixed layer leading to larger SSTA variability
112 (departures from the seasonal mean) in summer compared with winter.

113 In the vertical plane the wind-driven upper ocean circulation consists of a shallow
114 meridional overturning circulation, the subtropical cell (STC, Figure 5a). In the
115 subtropics and midlatitudes, water subducts, i.e. it leaves the mixed layer via downward
116 Ekman pumping and lateral induction via horizontal advection across the sloping base of
117 the mixed layer, and enters the main thermocline (Figure 5b). It flows downward and
118 equatroward along isopycnal surfaces where some of the water: *i)* returns to midlatitudes

via the southern and western branches of the subtropical gyre, *ii)* reaches the western boundary equatorward of ~20°S, and then flows towards the tropics and then eastward along the equator or *iii)* has a convoluted pathway in the ocean interior (Figure 5b). Water in *ii)* and *iii)* upwells at the equator, and then returns to the subtropics in the thin surface Ekman layer (Figure 5a). Observations [*Huang and Qiu*, 1994; *Johnson et al.*, 1999], modeling studies [*McCreary and Lu*, 1994; *Liu,* 1994; *Qu et al.,* 2002] and analyses of transient tracers such as tritium from nuclear bomb tests [*Fine et al.*, 1981; *Fine et al.*, 1983], suggest that subduction zones in the North Pacific contribute much of the water within the equatorial undercurrent which then reaches the surface in the eastern equatorial Pacific. Thus, variations in the temperature or strength of this cell could alter conditions in the equatorial Pacific on decadal time scales including modulating ENSO variability.

3) SST TENDENCY SURFACE HEAT BUDGET

Following *Frankingoul* [1985], the SST tendency equation, derived by integrating the heat budget over the mixed layer (ML), can be written as:

$$\frac{\partial T_m}{\partial t} = \frac{Q_{net}}{\rho_o c_p h} + \left(\frac{w + w_e}{h}\right)\left(T_b - T_m\right) - \boldsymbol{v}\cdot\nabla T_m - \frac{Q_{swh}}{\rho_o c_p h} + A\nabla^2 T_m \qquad (1)$$

I II III IV V

where T_m is the ML temperature, which is equivalent to the SST for a well mixed surface layer, Q_{net} the net surface heat flux, ρ_o and c_p are the density and specific heat of ocean

141 water, w the mean vertical motion, w_e the entrainment velocity – the turbulent flux
142 through the base of the ML, T_b the temperature just below the ML, $\boldsymbol{v}$ the horizontal
143 velocity, Q_{swh} the penetrating solar radiation at h and A the horizontal diffusion
144 coefficient. The terms in Equation 1 are: I) surface heating/cooling; II) vertical
145 advection/mixing; III) horizontal advection; IV) sunlight exiting the base of the mixed
146 layer and V) horizontal diffusion due to eddies.

147 The net surface heat exchange has four components: the shortwave (Q_{sw}), longwave
148 (Q_{lw}), sensible (Q_{sh}) and latent (Q_{lh}) heat fluxes. Variability in the sensible and latent heat
149 fluxes, which are functions of the near surface wind speed, air temperature and humidity,
150 and SST, dominate Q_{net} in winter, since the atmospheric internal variability and mean air-
151 sea temperature difference is much larger during the cold season. Anomalies in Q_{lh} and
152 Q_{sh} are about the same magnitude at high latitudes, while $Q_{lh} >> Q_{sh}$ in the tropics and
153 subtropics, since warm air holds more moisture and small changes in temperature can
154 lead to large changes in specific humidity (the relative humidity is nearly constant at
155 about 75-80% over the ocean). Anomalies in Q_{sh} and Q_{lh} are primarily associated with
156 wind speed anomalies in the tropics and subtropics but are more dependent on
157 temperature and humidity anomalies at mid to high latitudes. In general, Q_{lw}, varies less
158 than the other three components but is generally in phase with the latent and sensible
159 flux. Fluctuations in cloudiness, especially stratiform clouds, have a strong influence on
160 Q_{sw} over the North Pacific in spring and summer.

161 In the open ocean, the vertical mass flux into the mixed layer is primarily due to
162 entrainment [*Frankignoul*, 1985; *Alexander*, 1992a], i.e. $w_e > w$, although the latter is
163 critical for driving the ocean circulation. The ML deepens via entrainment; anomalies in

w_e are primarily generated by wind stirring in summer and surface cooling in fall and winter [*Alexander et al.*, 2000]. The mixed layer shoals by reforming closer to the surface; there is no entrainment at that time ($w_e = 0$) and h is the depth at which there is a balance between surface heating (positive buoyancy flux), wind stirring and dissipation. In general, deepening occurs gradually over the cooling season while the mixed layer shoals fairly abruptly in the spring. Anomalies in h can impact the heat balance of the ML especially in spring and summer: if the ML shoals earlier than usual, the average net heat flux will heat up the thinner surface layer more rapidly, creating positive SST anomalies [*Elsberry and Garwood*, 1978].

Horizontal temperature advection is primarily due to Ekman ($\boldsymbol{\nu}_{ek}$) and geostrophic ($\vec{v}_g$) currents, although ageostrophic currents associated with eddy activity also impact SST in coastal regions and near western boundary currents. The integrated Ekman transport over the mixed layer is given by $\boldsymbol{\nu}_{ek} = -\boldsymbol{k} \times \boldsymbol{\tau} / \rho_o f$, i.e. it is 90º to the right of the surface wind stress in the Northern Hemisphere. The large-scale currents in the North Pacific are in geostrophic balance and are part of the subtropical and subpolar gyres.

The contribution of the terms in Equation 1 to SSTA varies as a function of location, season, and time scale. Q_{net} variability in term I) is an important component of the heat budget over most of the Northern Hemisphere oceans from submonthly to decadal timescales and throughout the seasonal cycle. Entrainment impacts SSTA directly via the heat flux through the base of the mixed layer (II) and indirectly through its control of h (in I, II and IV), which have their greatest impact on SSTA in fall and spring respectively. Since Ekman currents respond rapidly to changes in the wind, they have nearly an instantaneous impact on SSTA (in III), but can contribute to interannual and

longer time-scale scale variability if the wind or SST gradient anomalies are long lived. Ekman advection contributes to SSTA along the subpolar front and in the central Pacific where strong zonal wind anomalies create anomalous meridional Ekman currents perpendicular to the mean SST gradient. Changes in the large-scale wind fields over the North Pacific generate oceanic Rossby waves that slowly propagate westward. The associated changes in $\boldsymbol{v}_g$ and the position and strength of the gyres, impact SSTs on decadal time scales especially in the KE region. Penetrating solar radiation (IV) and horizontal diffusion (V) are relatively small and the latter acts to damp SSTA. For more detailed analyses of the terms contributing to North Pacific SSTA see [*Frankignoul and Reynolds,* 1983; *Frankignoul,* 1985; *Cayan 1992a,b,c; Miller et al.*, 1994; *Alexander et al.* 2000; *Qiu*, 2000, and *Seager et al.,* 2001].

4) PROCESSES THAT GENERATE MIDLATIUDE SSTA (PACIFIC FOCUS)

Equation 1 can be used to interpret theoretical and numerical models of the upper ocean that increase in complexity as more terms on the right hand side are included. For a motionless ocean with fixed depth *h*, the temperature (SST) tendency is given by I; the SST behavior in such a slab ocean can be quite complex given the simplicity of the model. Including Term II allows for vertical processes in the ocean, which have been simulated by integral mixed layer models that predict *h*, or layered models that have vertical diffusion between layers. While the Ekman term in III can be represented via heat flux forcing of the mixed layer, the broader impact of currents have been considered from relatively simple shallow water models to full physics regional and general circulation models (GCMs).

4.1 *Stochastic forcing*

Hasselmann [1976] proposed that some aspects of climate variability could be represented by a slow system that integrates random or stochastic forcing. Like particles undergoing Brownian motion, the slow climate system exhibits random walk behavior, where the variability increases (decreases) with the square of the period (frequency). *Frankignoul and Hasselmann* [1977] were the first to apply a stochastic model to the real climate system in a study of midlatitude SST variability. The ocean was treated as a motionless slab where the surface heat flux both forces and damps SST anomalies. The forcing represents the passage of atmospheric storms, where the rapid decorrelation time between synoptic events results in a nearly white spectrum (constant as a function of frequency) over the evolution time scale of SST anomalies. The system is damped by a linear negative air-sea feedback, which represents the enhanced (reduced) loss of heat to the atmosphere from anomalously warm (cold) waters and vice-versa. The model may be written as:

$$\rho ch \frac{dT_m'}{dt} = F' - \lambda T_m' \qquad (2)$$

where a $'$ denotes a departure from the time mean, F' is the stochastic atmospheric forcing (constant for white noise) and λ the linear damping rate whose inverse gives the decay time. The stochastic model is characterized as a first order autoregressive, AR1, where the predictable part of T_m' (equivalent to SST) depends only on its value at the previous time. The auto correlation (r) of an AR1 process decays exponentially, i.e.,

$$r(\tau) = \exp\left[-\lambda\tau/\rho ch\right], \qquad (3)$$

where τ is the time lag.

The forcing and damping values can be estimated through several different means. If one assumes that the forcing and feedback are entirely through the net heat flux in nature then, F' can be obtained from the Q_{net} variance [*Czaja*, 2003], from simple models of the variables in the bulk formulas [*Frankignoul and Hasselmann*, 1977; *Alexander and Penland*, 1996], or indirectly from the SST variance [*Reynolds,* 1978;]. The damping coefficient can be estimated from the SST autocorrelation (e.g. inverting Equation 3), using typical values in the bulk aerodynamic flux formulas [*Lau and Nath*, 1996], the flux response in atmospheric general circulation model (AGCM) experiments to specified SSTAs [*Frankignoul*, 1985], or from the covariance between T_m and Q after removing the ENSO signal [*Frankignoul and Kestnare*, 2002; *Park et al.*, 2005]. Typical λ^{-1} values obtained from these methods are 2-6 months, which corresponds to a flux damping of 10-40 $\text{Wm}^{-2}\ ^{\circ}\text{C}^{-1}$, over most of the North Pacific.

The variance spectrum of T_m' from Equation 2 may be written as:

$$\left|T_m'(\omega)\right|^2 = \frac{\left|F'\right|^2}{\omega^2 + \lambda^2}, \tag{4}$$

where ω is the frequency and $|\ |^2$ indicates the variance or power spectrum. At short time scales or high frequencies ($\omega >> \lambda$), the ocean temperature variance increases with the square of the period (slope of -2 in a log-log spectral plot, Figure 6). At longer time scales ($\omega << \lambda$), the damping becomes progressively more important, and the spectrum asymptotes as negative air-sea feedback limits the magnitude of the SST anomalies. This red noise spectrum contains variability on decadal and longer time scales but without spectral peaks. The Hasselmann model has been quite effective at describing the temporal

255 variability of mid-latitude SST variability in numerous observational (e.g. Figure 6) and
256 modeling studies, and should be considered as the null hypothesis for extratropical SST
257 variability.

258 Several refinements/extensions have been proposed to the stochastic model for
259 midlatitude SSTs:

260 a) The inclusion of additional processes, such as the rapidly varying portions of the
261 Ekman transport and entrainment in the stochastic forcing [*Frankignoul*, 1985,
262 *Dommenget and Latif*, 2002; *Lee et al.*, 2008]

263 b) The forcing and feedback are cyclostationary, i.e. F and λ vary with the seasonal
264 cycle [*Frankignoul*, 1985: *Ortiz and Ruiz de Elvira*, 1985; *Park et al.*, 2006].

265 c) The damping coefficient is given by $\lambda = \langle\lambda\rangle + \lambda'$, where $\langle\lambda\rangle$ is constant but λ'
266 varies rapidly and can be approximated by white noise. As a result there is a second,
267 "multiplicative noise" term that depends upon the SST anomaly ($\lambda' T_m'$). Rapid
268 fluctuations in λ', via wind gusts, can significantly contribute to the overall stochastic
269 forcing [*Sura et al.*, 2006].

270 d) Enabling air-sea feedback by using a second stochastic equation for surface air
271 temperature, which is thermodynamically coupled to the ocean via the air-sea
272 temperature difference [*Frankignoul*, 1985; *Barsugli and Battisti*, 1998]. With coupling,
273 the air temperature adjusts to the underlying SSTA reducing the thermal damping, which
274 significantly enhances the decadal SST variability but reduces the surface flux variability
275 (it approaches zero at long time scales) and is apparent when comparing AGCMs with
276 specified SSTs to those coupled to mixed layer ocean models [*Bladé*, 1997; *Bhatt et al.*,
277 1998; *Saravanan*, 1998].

The primary effect of these extensions to the Hasselmann model is to increase the SSTA variance at annual and longer time scales.

4.2 Cloud-SST feedbacks

Both the insolation and the amount of stratiform clouds are greatest over the North Pacific in summer. Increased clouds cool the ocean, while a colder ocean enhances the static stability, leading to more stratiform clouds that reduce Q_{sw} [*Norris and Leovy*, 1994; *Weare*, 1994; *Klein et al.*, 1995;]. This positive feedback occurs over the central and western Pacific at ~40°N where there are strong gradients in both SST and cloud amount [*Norris et al.*, 1998]. The positive SST-low cloud feedback increases the persistence of North Pacific SST anomalies during the warm season [*Park et al.*, 2006].

4.3 "The Reemergence Mechanism"

Seasonal variations in h have the potential to influence the evolution of upper ocean thermal anomalies. *Namias and Born* [1970, 1974] were the first to note a tendency for midlatitude SST anomalies to recur from one winter to the next without persisting through the intervening summer. They speculated that temperature anomalies that form at the surface and spread throughout the deep winter mixed layer remain beneath the mixed layer when it shoals in spring. The thermal anomalies are then incorporated into the summer seasonal thermocline where they are insulated from surface fluxes that damp anomalies in the mixed layer. When h deepens again in the following fall, the anomalies are re-entrained into the surface layer and influence the SST. *Alexander and Deser* [1995] termed this process the "reemergence mechanism" (shown schematically in Figure 3) and

301 it has been documented over large portions of the North Atlantic and North Pacific
302 Oceans using subsurface temperature data and mixed layer model simulations [*Alexander*
303 *et al.*, 1999; 2001; *Bhatt et al.*, 1998; *Watanabe and Kimoto*, 2000; *Timlin et al.*, 2002;
304 *Hanawa and Sugimoto*, 2004].

305 The evolution of upper ocean temperatures in three North Pacific regions is shown by
306 regressing the temperature anomalies as a function of month and depth on SST anomalies
307 in April-May (Figure 7). The regressions depict how a 1°C SSTA in spring linearly
308 evolves from the previous January through the following April. The regressions indicate
309 the reemergence mechanism occurs in the east, central and west Pacific: the anomalies
310 which extend through out the deep winter mixed layer are maintained beneath the surface
311 in summer and then return to the surface in the following fall and winter. The regional
312 differences in the timing and strength of the reemergence mechanism are partly due to
313 variations in the seasonal cycle of h across the North Pacific. The maximum h, which
314 tends to occur in March, increases from about 80 m along the west coast of North
315 America, to 120 m in the central Pacific and 150-250 m in the west Pacific (Figure 4).

316 Combining the Hasselmann model with one that includes the seasonal cycle of h
317 significantly enhances the winter-to-winter autocorrelation of SST anomalies via the
318 reemergence mechanism [*Alexander and Penland*, 1996; *Deser et al.*, 2003]. The lag
319 autocorrelation of North Pacific SSTA starting from March indicates a clear annual cycle
320 with peaks in March of successive years, due to the reemergence mechanism, while the
321 total heat content (including the temperature anomalies in the summer thermocline)
322 appears to decay at a constant rate, as expected from the Hasselmann model that uses the
323 winter h to calculate the damping rate. This indicates that the winter mixed layer depth

should be used when calculating the feedback parameter λ for studies of the year-to-year persistence of SST anomalies.

4.4 *Dynamic ocean process*

Ocean dynamics, including advection (Term III), allows for additional mechanisms that contribute to SST variability on interannual and decadal times. Since currents advect ocean temperature anomalies, the reemergence process can be non-local, i.e. SST anomalies created in one winter may return to the surface at a different location in the subsequent winter. Remote reemergence is pronounced in regions of strong currents such as the Gulf Stream [*de Coëtlogon and Frankignoul*, 2003] and Kuroshio Extension [*Sugimoto and Hanawa*, 2005]. In the latter, anomalies created near Japan propagate to the central Pacific by the following winter.

Saravanan and McWilliams [1997, 1998] proposed the "advective resonance" hypothesis where a decadal SSTA peak can be generated based only on the spatial structure of atmospheric forcing and a constant ocean velocity. For interannual and longer periods extratropical atmospheric variability tends to be dominated by fixed spatial patterns that are white in time. Stochastic forcing by these large-scale patterns can lead to low frequency variability if the forcing has a multi-pole structure and the ocean advection traverses the centers of the poles. A simple model of such a system devised by Saravanan and McWilliams has two regimes, one where thermal damping dominates ocean advection and the other where advection dominates. In the former, the oceanic and atmospheric power spectra are slightly reddened, but do not show any preferred periodicities. While in the latter, the overall variance in the atmosphere and ocean

decreases, but a well defined periodicity corresponding to the timescale emerges given by the length scale of the atmospheric forcing divided by the ocean velocity. *Wu and Liu* [2003] found that advective resonance could generate decadal variability in the eastern North Pacific but the SST anomalies were initiated by Ekman transport rather than the net heat flux.

The dynamic adjustment of upper-ocean gyre circulation primarily occurs via westward propagating Rossby waves forced by anomalous wind stress. The relevant equation for wind forced waves can be written as [see *Dickinson*, 1987; *Gill*, 1982]:

$$\frac{\partial h_t}{\partial t} + c\frac{\partial h_t}{\partial x} = \frac{1}{\rho_0 f}\nabla x\boldsymbol{\tau} - \varepsilon h_t \qquad (5)$$

where h_t is the depth of the thermocline, c is the speed of the 1st baroclinic mode Rossby wave, the constant ρ_0 is the sea water density, f is the Coriolis parameter, $\nabla x\boldsymbol{\tau}$ is the wind stress curl which drives vertical motion, via Ekman pumping and ε is a damping coefficient. h_t anomalies are generally compensated by perturbations in the sea surface height (SSH, e.g. *Gill* 1982), which can be measured from satellite [e.g. *Robinson*, 2004]. Rossby waves generated by large-scale wind forcing are long and thus non-dispersive, i.e. their speeds are independent of wavelength. The Rossby waves propagate nearly due west along a latitude circle (Figure 8), where c decreases rapidly with latitude. The large-scale Rossby wave response (Figure 8b) results from the integrated $\nabla x\boldsymbol{\tau}$ forcing, producing maximum SSH (h_t) variability near the western boundary, while the full SSH

field includes small-scale structures associated with eddies in the KE region (Figure 8a). The dominant time scale of the large-scale response is set by the basin width, the spatial scale and location (relative to the western edge) of the atmospheric forcing, and the Rossby wave speed. At the latitude of the Kuroshio Extension (35ºN) c is ~2.5 cm s^{-1}. For a basin the size of the Pacific, the adjustment timescale is on the order of ~5 (10) years if the Rossby wave was initiated in the central (far eastern) Pacific.

The Hasselman model can also be used to understand the dynamical ocean response to wind forcing. Rossby waves excited by stochastic $\nabla x\boldsymbol{\tau}$ forcing that is zonally uniform produces a h_t spectrum that increases with period but then reaches constant amplitude at low frequencies [*Frankignoul et al.*, 1997]. When the forcing has a more complex structure, such as sinusoidal waves in the zonal direction, decadal peaks can occur in the spectra due to resonance with the basin-scale Rossby waves [*Jin*, 1997], which is equivalent to the advective resonance mechanism but where the anomaly pattern propagates via Rossby waves rather than by the mean currents. Decadal peaks may also result from the reduction in Rossby wave speed as the latitude increases: wind forcing at in the central Pacific creates westward Rossby waves that result in h_t anomalies of opposite sign on either side of the Kuroshio on ~10 year time scales [*Qiu*, 2003]. The gradient of h_t influences the strength of the jet via geostrophic adjustment.

The gyre adjustment process impacts SSTs through changes in thermocline depth and the currents. Given the westward deepening of the mixed layer across the basin between 30°-50°N in winter (Figure 4), fluctuations in the upper thermocline are well below h in the central Pacific but close to the base of the mixed layer in the western Pacific. Thus, when Rossby waves propagate into the KE region in winter the associated temperature

anomalies can then be mixed to the surface via local turbulence. *Schneider and Miller* [2001] were thereby able to predict winter SSTA in the KE region several years in advance using the Rossby wave model (Eq. 5), forced with the observed $\nabla x\boldsymbol{\tau}$, plus a local linear regression between h_t and SST in the KE region. Anomalies in h_t and SST are relatively independent in summer and over most of the North Pacific in the KE region in all seasons.

Once the h_t anomalies propagate into the west Pacific, the position and strength of the KE changes [e.g. *Qiu*, 2000; *Kelly, 2004*; *Qiu and Chen*, 2005], which also impacts SSTs along ~40°N due to anomalous geostrophic heat transport [*Seager et al.*, 2001; *Schneider et al.*, 2002, *Dawe and Thompson* 2007; and *Kwon and Deser*, 2007; *Qiu et al.*, 2007]. Satellite altimetry data and high resolution ocean models indicate that the large scale flow resulting from the arrival of Rossby waves affect the strength of the front and eddy activity in the KE region [*Qiu and Chen,* 2005; *Taguchi et al.,* 2005; 2007], where the resulting ageostrophic currents influence SSTA [*Dawe and Thompson*, 2007].

4.5 Midlatitude air-sea interaction

While atmospheric forcing was crucial in generating low-frequency variability in the aforementioned studies, they did not require an atmospheric response to the developing ocean anomalies. Coupled feedbacks could enhance or give rise to new midlatitude modes of decadal variability. Based on analyses of a coupled atmosphere ocean GCM, *Latif and Barnett* [1994, 1996] proposed a feedback loop between the strength of the Aleutian Low and the subtropical ocean gyre circulation to account for the presence of decadal oscillations. They argued that an intensification of the Aleutian Low would

415 strengthen the subtropical gyre after a delay associated with the Rossby wave adjustment
416 process. An anomalously strong subtropical gyre transports more warm water into the
417 Kuroshio Extension, leading to positive SST anomalies in the western and central North
418 Pacific. In their coupled model experiment and in supplementary AGCM simulations
419 with prescribed SSTA, the atmosphere was very sensitive to SST variations in the KE
420 region, where a strong anomalous high developed over the central Pacific in response to a
421 positive SST anomalies in the KE. The circulation around the high advected warm moist
422 air-over the positive SSTA, which maintained the SST anomalies but reduced the
423 strength of the Aleutian Low, which subsequently weakened the subtropical gyre,
424 switching the phase of the oscillation ~10 years later.

425 While many aspects of the Latif and Barnett hypothesis occur in nature, such as the
426 Rossby wave adjustment to $\nabla x \boldsymbol{\tau}$ anomalies associated with the strength of the Aleutian
427 low, some are not consistent with data and ocean model simulations driven by observed
428 atmospheric conditions. In particular, when the Aleutian Low strengthens it also shifts
429 southward, as a result, the gyre circulation shifts equatorward and the SST anomalies
430 subsequently cool rather than warm in the KE region [Figure 9; *Deser et al*., 1999, *Miller*
431 *and Schneider*, 2001; *Seager et al.,* 2001] as discussed further in section 5.2.3. In
432 addition, rather than a positive thermal air-sea feedback, surface heat fluxes damps SST
433 anomalies in the KE region both in observations and ocean model hindcasts [*Seager et*
434 *al.,* 2001; *Tanimoto et al*., 2003; *Kelly*, 2004]. Finally, the atmospheric response in the
435 AGCM simulations conducted by Latif and Barnett were much larger than in nearly all
436 other AGCM experiments [see *Kushnir et al.*, 2002].

While the original Latif and Barnett mechanism may not be fully realized, midlatitude ocean-to-atmosphere feedbacks still appear to influence decadal variability. Observations, theoretical models and coupled GCMs suggest there is positive air-sea feedback in the North Pacific [*Weng and Neelin*, 1999; *Schneider et al.*, 2002; *Wu et al.*, 2005; *Kwon and Deser*, 2007; *Frankignoul and Sennéchael*, 2007; *Qiu et al.*, 2007]. As in the original Latif and Barnett hypothesis wind stress curl anomalies in the central Pacific generates ocean Rossby waves that lead to adjustment of the ocean gyres ~5 years later (Figure 9a), but in contrast to Latif and Barmett, the SST anomalies in the Kuroshio region are maintained by geostrophic currents due to a change in the position of the gyre (Figure 10) and to some extent the Ekman transport, rather than surface fluxes. When the gyres shifts north, KE SSTs increase and the upward directed latent heat fluxes lead to enhanced precipitation over the KE region and, in some model experiments, a broader atmospheric response that includes $\nabla x \boldsymbol{\tau}$ anomalies over the central North Pacific that are similar in structure but opposite in sign and somewhat weaker than the curl anomalies reversing the sign of the oscillation forcing pattern (Figure 9b). While this coupled feedback loop explains a small amount of the overall SST variance, it produces a modest spectral peak above the red noise background on decadal time scales [*Kwon and Deser*, 2007; *Qiu et al.*, 2007].

4.6 Tropical-extratropical interactions

Variability in the North Pacific may not only be generated by extratropical processes but also arise due to fluctuations originating in the tropics that are communicated to

459 midlatitudes by the atmosphere and/or ocean. Furthermore, two-way interactions between
460 the tropical and North Pacific may impact low-frequency variability in both domains.
461
462 4.6.1 "The Atmospheric Bridge" (ENSO Teleconnections)
463 ENSO-driven atmospheric teleconnections [*Trenberth et al.*, 1998; *Liu and*
464 *Alexander*, 2007, chapter 7] alter the near-surface air temperature, humidity, wind and
465 clouds far from the equatorial Pacific. The resulting variations in the surface heat,
466 momentum and fresh water fluxes cause changes in SST, *h*, salinity, and ocean currents.
467 Thus, the atmosphere acts like a bridge spanning from the equatorial Pacific to the North
468 Pacific, South Pacific, the North Atlantic and Indian Oceans [e.g. *Alexander*, 1990,
469 1992a; *Lau and Nath*, 1994, 1996, 2001; *Klein et al.*, 1999; *Alexander et al.*, 2002]. The
470 SST anomalies that develop in response to this "atmospheric bridge" may feed back on
471 the original atmospheric response to ENSO.
472 When El Niño events peak in boreal winter, enhanced cyclonic circulation around the
473 deepened Aleutian low (Plate 1a) results in anomalous northwesterly winds that advect
474 relatively cold dry air over the western/central North Pacific, anomalous southerly winds
475 that advect warm moist air along the west coast of North America and enhanced surface
476 westerlies over the central North Pacific. The resulting anomalous surface heat fluxes and
477 Ekman transport create negative SSTA between 30ºN-50ºN west of ~150ºW and positive
478 SSTA along the west coast of North America (Plate 1a; *Alexander et al.,* 2002; *Alexander*
479 *and Scott*, 2008]. In the central North Pacific, the stronger wind stirring and negative
480 buoyancy forcing due to surface cooling increases the *h* through the winter and some of

481 the anomalously cold water returns to the surface in the following fall/winter via the
482 reemergence mechanism [*Alexander et al.*, 2002].

483 Studies using AGCM-mixed layer ocean model simulations have confirmed the
484 basic bridge hypothesis for forcing North Pacific SST anomalies, but have reached
485 different conclusion on the impact of these anomalies on the atmosphere [*Alexander*,
486 1992b; *Bladé*, 1999; *Lau and Nath*, 1996, 2001]. More recent model experiments suggest
487 that the oceanic feedback on the extratropical response to ENSO is complex, but of
488 modest amplitude, i.e. atmosphere-ocean coupling outside of the tropical Pacific slightly
489 modifies the extratropical atmospheric circulation anomalies but these modifications
490 depend on the seasonal cycle and air-sea interactions both within and beyond the North
491 Pacific Ocean [*Alexander et al.*, 2002; *Alexander and Scott,* 2008].

492 Most studies of the atmospheric bridge have focused on boreal winter since
493 ENSO and the associated atmospheric circulation anomalies peak at this time. However,
494 significant bridge-related changes in the climate system also occur in other seasons. Over
495 the western North Pacific, the southward displacement of the jet stream and storm track
496 in the summer prior to when ENSO peaks changes the solar radiation and latent heat flux
497 at the surface, which results in anomalous cooling and deepening of the oceanic mixed
498 layer at ~40ºN [*Alexander et al.*, 2004; *Park and Leovy*, 2004]. The strong surface flux
499 forcing in conjunction with the relatively thin mixed layer in summer leads to the rapid
500 formation of large-amplitude SST anomalies in the Kuroshio Extension (Plate 1b).

501 While the atmospheric bridge primarily extends from the tropics to the extratropics,
502 variability originating in the North Pacific may also influence the tropical Pacific. *Barnett*
503 *et al.* [1999] and *Pierce et al*. [2000] proposed that the atmospheric response to slowly

504 varying SST anomalies in the Kuroshio Extension region, extends into the tropics,
505 thereby affecting the trade winds and decadal variability in the ENSO region. *Vimont et*
506 *al*. [2001, 2003] found that the extratropical atmosphere can generate tropical variability
507 via the "seasonal footprinting mechanism". Large fluctuations in the North Pacific
508 Oscillation, an intrinsic mode of atmospheric variability, impart an SST footprint onto the
509 ocean during winter via changes in the surface heat fluxes, which persists through
510 summer in the subtropics, and impacts the atmospheric circulation including zonal wind
511 stress anomalies that extend onto and south of the equator. These wind stress anomalies
512 are an important element of the stochastic forcing of interannual and decadal ENSO
513 variability [*Vimont et al.*, 2003; *Alexander et al.*, 2008].
514
515 4.6.2 Ocean teleconnections
516 The equatorial thermocline variability associated with ENSO excites Kelvin and other
517 coastally trapped ocean waves, which propagate poleward along the eastern Pacific
518 boundary in both hemispheres, generating substantial sea level variability [*Enfield and*
519 *Allen*, 1980; *Chelton and Davis*, 1982; *Clarke and van Gorder*, 1994]. However, these
520 waves impact the ocean only within ~50 km of shore north of 15°N [*Gill*, 1982]. Energy
521 from the coastal waves can also be refracted as long Rossby waves that propagate
522 westward across the extratropical Pacific [*Jacobs et al.*, 1994; *Meyers et al.*, 1996].
523 However, wind forcing rather than the eastern boundary waves appears to be the
524 dominant source of Rossby waves across much of the North Pacific [*Miller et al.*, 1997;
525 *Chelton and Schlax*, 1996; *Fu and Qiu*, 2002].
526 *Gu and Philander* [1997] proposed a mechanism for decadal variability that relies on

527 the subduction of surface temperature anomalies in the North Pacific and their subsequent
528 southward propagation in the lower branch of the STC. Upon reaching the equator the
529 thermal anomalies upwell to the surface and amplify via interactions between the zonal
530 wind, SST gradient and upwelling, known as the "Bjerknes feedback" (e.g. see Neelin et
531 al. 1998) and subsequently influence the North Pacific via the atmospheric bridge. If
532 warm water is subducted, the subsequent positive anomalies on the equator will act to
533 strengthen the Aleutian Low, which creates cold anomalies in the central North Pacific
534 (Plate 1). This describes one half of the oscillation, the period of which is controlled by
535 the time it takes the water parcels to travel from the surface in the extratropics to the
536 equator. While observations show evidence of thermal anomalies subducting in the main
537 thermocline in the central North Pacific [*Deser et al.*, 1996; *Schneider et al.*, 1999], these
538 anomalies decay away from the subduction region, and the thermocline variability found
539 equatorward of 18° appears to be primarily associated with tropical wind forcing
540 [*Schneider et al., 1999*; *Capotondi et al.*, 2003]. SSTs in the equatorial Pacific, however,
541 may still be influenced by subduction and transport from the South Pacific [*Luo and*
542 *Yamagata*, 2001].

543 An alternate subduction-related hypothesis is that changes in the subtropical winds
544 alter the speed of the STC, thus changing the rate at which relatively cold water from the
545 surface layer in the extratropics is transported southward and then upwells at the equator.
546 Using an atmosphere-ocean model of intermediate complexity, *Kleeman et al.* [1999]
547 found that decadal variations of tropical SSTs could be induced by changes in the
548 subtropical winds, while the observational analyses of *McPhaden and Zhang* [2002]
549 indicated that slowing of the STCs in both hemispheres after 1970 relative to the previous

two decades, reduced upwelling along the equator and resulted in substantially warmer SSTs in the central equatorial Pacific.

4.6.3 *Two-way connections*

Liu et al. [2002] and *Wu et al.* [2003] performed sensitivity experiments using "model surgery" in which ocean-atmosphere interaction can be turned on and off in different regions. These experiments suggest that decadal variability arises in the tropical and North Pacific, via independent mechanisms but variability in both basins can be enhanced by tropical-extratropical interactions. For example, tropical Pacific decadal SST variance is almost doubled when extratropical ocean-atmosphere interaction and oceanic teleconnections are enabled. Observational [*Newman*, 2007] and modeling studies [*Solomon et al.*, 2003, 2008] support the concept of two-way coupling where variability in the North Pacific influences tropical low-frequency variability and vice-versa.

5) THE PACIFIC DECADAL OSCILLATION

5.1 pattern and temporal variability

The leading pattern of North Pacific monthly SST variability, as identified by empirical orthogonal function (EOF) analysis and the corresponding principal component (PC 1), the time series of the amplitude and phase of EOF 1, are shown in Figure 11. The time series (after removing the global mean temperature) has been termed the Pacific Decadal Oscillation (PDO) by Mantua et al. (1997) due to its low frequency fluctuations. The PDO underwent rapid transitions between relatively stable states or "regime changes" around 1925, 1947 and 1976, although interannual variability is also apparent in

573 the PDO time series. In the North Pacific, the PDO pattern has anomalies of one sign in
574 the central and western North Pacific between approximately 25°-45°N that are ringed by
575 anomalies of the opposite sign. However, the associated SST anomalies extend over the
576 entire basin and are symmetric about the equator [*Zhang et al.*, 1997; *Garreaud and*
577 *Battisti*, 1999], leading some to term the phenomenon the Interdecadal Pacific Oscillation
578 (IPO; *Power et al.*, 1999; *Folland et al.*, 2002].

579 The decadal SST transitions were accompanied by widespread changes in the
580 atmosphere, ocean and marine ecosystems [e.g. *Miller et al.*, 1994; *Trenberth and*
581 *Hurrell*, 1994; *Benson and Trites*, 2002; *Deser et al.*, 2004]. For example, *Mantua et al*.
582 [1997] found that timing of changes in the PDO closely corresponded to those in salmon
583 production along the west coast of North America. The positive phase of the PDO, with
584 cold water in the central Pacific and warm water along the coast of North America is
585 accompanied by a deeper Aleutian low, with negative SLP anomalies over much of the
586 North Pacific (Figure 11), warm surface air temperature over western North America and
587 enhanced precipitation over Alaska and the southern US and reduced precipitation across
588 the northern US/southern Canada [*Mantua et al.*, 1997; *Deser et al.*, 2004].

589

590 5.2 *Mechanisms for the PDO*

591 The PDO could be a critical factor in long-range forecasts given its long time scale
592 and connection to many important climatic and biological variables. However, this
593 depends on whether the mechanism(s) underlying the PDO is (are) predictable and the
594 relationship between PDO SSTA and the associated large-scale atmospheric circulation,
595 i.e. is the PDO *i)* driving, *ii)* responding to or *iii)* coupled with the later? We will expand

596 on the processes underlying midlatitude SST variability discussed in section 4 as
597 potential mechanisms for the PDO.
598
599 5.2.1 Fluctuations in the Aleutian Low (large-scale stochastic forcing)
600 The Hasselmann model for SSTs at a given location can be extended to understand
601 basin-wide SST anomaly patterns. *Frankignoul* and *Reynolds* [1983] found that white
602 noise forcing associated with large-scale atmospheric fluctuations could explain much of
603 the variability over the entire North Pacific, while *Cayan* [1992b] and *Iwasaka and*
604 *Wallace* [1995] found that interannual variability in the surface fluxes and SSTs are
605 closely linked to the dominant patterns of atmospheric circulation over the North Pacific
606 and North Atlantic Oceans. We explore SLP/Q_{net}/SST relationships using an AGCM
607 coupled to a variable depth ocean mixed layer model (MLM), with no ocean currents and
608 hence no ENSO variability or ocean gyre dynamics. As in nature, the leading pattern of
609 SLP variability over the North Pacific is associated with fluctuations in the Aleutian Low
610 (Figure 12a). The near-surface circulation around a stronger low, results in enhanced
611 wind speeds and reduced air temperature and humidity along ~35°N, which cools the
612 underlying ocean via the surface heat fluxes, while the northward advection of warm
613 moist air heats the ocean near North America. The structure of the SLP-related surface
614 flux anomalies (Figure 12b) is very similar to the dominant surface flux and SST patterns
615 (Figure 12c,d). Given that the model has no ocean currents and similar SLP and flux
616 patterns are found in AGCM simulations with climatological SSTs as boundary
617 conditions [*Alexander and Scott*, 1997], indicates that fluctuations in the Aleutian Low
618 can drive PDO-like SST anomalies via the surface flux field.

619 The temporal characteristics of the PDO are also consistent with the Hasselman
620 model, i.e. it exhibits a red noise spectrum without significant spectral peaks other than at
621 the annual period (Figure 13). *Pierce* [2001] generated 100-year synthetic time series
622 using a random number generator and the same lag one autocorrelation coefficient as the
623 observed PDO. The synthetic time series exhibited similar low-frequency variability as
624 the observed PDO with strings of years of the same sign separated by abrupt "regime
625 shifts" and exhibit "significant" (at the 95% level) spectral peaks but at different periods.
626 These findings suggest caution in attributing physical meaning to regime shifts and
627 spectral peaks even in century long data sets.
628
629 5.2.2 Teleconnections from the tropics
630 *Mantua et al.* [1997] noted that the PDO had only a modest correlation with ENSO
631 and that the North Pacific variability was of greater amplitude and lower frequency than
632 that in the tropical Pacific. However, the atmospheric bridge to the North Pacific is
633 complex and is a function of season, lag and location [*Newman et al.*, 2003] and also
634 depends on the ENSO index, data set, etc. [*Alexander et al.*, 2008]. Furthermore, the
635 ENSO-related North Pacific SST anomaly pattern during winter (Plate 1a) clearly
636 resembles the PDO, while the summer ENSO signal (Plate 1b) also projects on the PDO
637 pattern, particularly in the western North Pacific. So, to what extent does ENSO and
638 tropical SSTs in general impact the PDO?
639 *Zhang et al.* [1997] utilized several analysis techniques to separate interannual ENSO
640 variability from a residual containing the remaining (> 7 yr) "interdecadal" variability.
641 The SSTA pattern based on low-pass filtered data is similar to the unfiltered ENSO

642 pattern, except it is broader in scale in the eastern equatorial Pacific and has enhanced
643 magnitude in the North Pacific relative to the tropics. The extratropical component
644 closely resembles the PDO. Other statistical methods of decomposing the data indicate
645 that at least a portion of the decadal variability in the PDO region is associated with
646 anomalies in the tropical Pacific [e.g. *Nakamura et al.*, 1997; *Mestas Nuñez* and *Enfield*
647 *1999*; *Alexander et al.*, 2008].

648 While the broad structure of the 1st EOF of SSTA in observations (Figure 11a) and
649 the AGCM-MLM (Figure 12d) are similar, the anomalies extend along ~40°N in nature
650 but slope southwestward from the central Pacific toward the south China Sea in the
651 model. This bias could be due to several factors, including the absence of ENSO/the
652 atmospheric bridge in the original AGCM-MLM simulations. In AGCM-MLM-TP_OBS
653 experiments, in which the MLM is coupled to the AGCM except in the tropical Pacific
654 where observed SSTs are prescribed for the years 1950-1999, the dominant pattern of
655 North Pacific SSTAs closely resembles the observed PDO [see Fig. 5 in *Alexander et al.*,
656 2002].

657 The observed difference between SSTs averaged over periods 1977-1988 and 1970-
658 1976 during winter includes warm ENSO-like conditions in the tropical Pacific and the
659 positive phase of the PDO in the North Pacific (Figure 14a). A comparable plot based on
660 an ensemble average of 16 AGCM-MLM-TP_OBS simulations has a similar pattern in
661 the North Pacific (Figure 14b), confirming that the atmospheric bridge can contribute to
662 low-frequency variability in the PDO, although the amplitude of the North Pacific
663 anomalies in the MLM are ~1/3 of their observed counterparts. While there is a wide
664 range in epoch differences between ensemble members (not shown), this estimate of

665 ENSO's impact on low-frequency PDO variability is consistent with that of *Schneider*
666 *and Cornuelle* [2005], discussed later in this section.

667 The influence of the tropics on decadal variability in the North Pacific variability via
668 the atmospheric bridge may occur via the teleconnection of decadal signals originating in
669 the ENSO region [*Trenberth*, 1990; *Graham et al.*, 1994; *Deser and Phillips*, 2006],
670 decadal forcing from other portions of the tropical Pacific and Indian Oceans [*Deser et*
671 *al.*, 2004; Newman, 2007] and/or by ENSO-related forcing on interannual time scales
672 which is integrated, or reddened by ocean processes in the North Pacific, including the
673 reemergence mechanism [*Newman et al.*, 2003; *Schneider and Cornuell*e, 2005].
674 *Alexander et al.* [1999, 2001] showed that the PDO pattern could recur in consecutive
675 winters via the reemergence mechanism.

676

677 5.2.3) Midlatitude ocean dynamics and coupled variability

678 The role of ocean dynamics in PDO variability has been investigated through the
679 change in ocean circulation that occurred in 1976-1977, when the ocean rapidly
680 transitioned from the negative to positive phase of the oscillation (Figure 11c). The
681 strengthening and southward displacement of the Aleutian low beginning in the winter of
682 1976 and in the decade that followed, cooled the central Pacific by enhanced Ekman
683 transport, vertical mixing and upward surface heat flux [*Miller et al.*, 1994]. This cooling
684 projected strongly on the PDO in the center of the basin. In addition, the maximum
685 westerly winds intensified and shifted from about 40°N to 35°N and hence $\nabla x\tau$ and
686 Ekman pumping shifted southward, with anomalous downward (upward) values south
687 (north) of 35°N (Figure 15a,b). Following the Rossby waves adjustment process to the

688 wind forcing (see section 4.4), the thermocline deepened (shoaled) south (north) of the
689 mean KE axis at ~35°N and the gyres strengthened and shifted southwards over a ~5 yr
690 period (Figure 15c,d). Geostrophic advection associated with southward gyre position,
691 strongly cooled the ocean along 40°N. The SST anomalies in the KE region, also project
692 onto the PDO, helping to maintain the positive phase of the PDO through the 1980s.
693 The 20-30 year persistence of anomalies in the PDO record and ~15-25 yr period of
694 PDO variability in paleoclimate reconstructions [*Biondi* et al., 2001; *Gedalof*, 2002] and
695 in some coupled GCM studies, has lead some to suggest that the PDO is due to positive
696 atmosphere-ocean feedbacks necessary to sustain decadal oscillations. While the North
697 Pacific Ocean appears to have the necessary dynamics to generate low frequency
698 variability, it is unclear whether the atmospheric response to the associated SST
699 anomalies has the correct spatial pattern, phase and amplitude for decadal oscillations. On
700 one hand, recent coupled GCM experiments [*Kwon and Deser*, 2007] and observationally
701 derived heuristic models [*Qiu et al.*, 2007] suggest that the atmospheric response to SST
702 anomalies in the Kuroshio extension region, while modest, is sufficiently strong to
703 enhance variability at decadal periods. On the other hand, the wind stress curl pattern
704 diagnosed as the response to the KE SST anomalies by *Kwon and Deser* [2007], was of
705 one sign across the Pacific at ~40°N, while *Qiu et al.* [2007] found that it switched signs
706 in the center of the basin. There are also conflicting results from AGCM studies with
707 either specified SST anomalies [e.g. *Peng et al.*, 1997; *Peng and Whitaker*, 1999] or
708 where the ocean component is a slab mixed layer and an anomalous heat source,
709 representing geostrophic heat flux convergence, is added in the KE region [*Yulaeva et al.*,
710 2001; *Liu and Wu*, 2004; *Kwon and Deser*, 2007]. Some models exhibit a baroclinic

711 response with a surface low that decrease with height downstream over the central
712 Pacific, while others have an equivalent barotropic response with a surface high that
713 increases with height over the central Pacific. The former is in direct response to the low-
714 level heating while the latter is stronger and driven by changes in the storm track. In
715 addition, most AGCM studies have found that the response to extratropical SSTs is
716 relatively small compared to internal atmospheric variability [*Kushnir et al.*, 2002],
717 although the current generation of coupled GCMs may not sufficiently resolve all of the
718 oceanic as well as atmospheric processes that could contribute to the PDO.
719
720 5.2.4 The PDO: a multi-process phenomena?
721 How can we reconcile these conflicting findings on the mechanism for the PDO?
722 Several recent studies have used statistical analyses to reconstruct the annually averaged
723 (July-June) PDO and determine the processes that underlie its dynamics. *Newman et al.*
724 [2003] found that the PDO is well modeled as the sum of atmospheric forcing represented
725 by white noise, forcing due to ENSO, and memory of SST anomalies in the previous year
726 via the reemergence mechanism. Expanding on this concept, *Schneider and Cornuelle*
727 [2005] found that the annually averaged PDO could be reconstructed based on an AR1
728 model and forcing associated with stochastic variability in the Aleutian low, ENSO
729 teleconnections, and shifts in the North Pacific Ocean gyres; vertical mixing of
730 temperature anomalies associated with wind-driven Rossby waves had little impact on
731 the PDO (Figure 16a). On interannual time scales, random Aleutian Low fluctuations and
732 ENSO teleconnections were about equally important in determining the PDO variability
733 with negligible contributions from ocean currents, while on decadal timescales, stochastic

734 forcing, ENSO and changes in the gyre circulations, each contributed approximately 1/3
735 of the PDO variance (Figure 16b). A key implication of these analyses is that, unlike
736 ENSO, the PDO is likely not a single physical mode but rather the sum of several
737 phenomena. Furthermore, random combinations of these and perhaps other processes
738 can give rise to apparent "regime shifts" in the PDO that are not predictable beyond about
739 two years [*Barlow et al*., 2001; *Schenider and Cornuelle*, 2005; *Alexander et al*., 2007;
740 *Newman*, 2007].
741
742 6) BEYOND THE PDO
743 The PDO is only one measure of variability in the North Pacific, it is possible that
744 other regions and/or modes of variability may primarily result from North Pacific
745 atmosphere-ocean dynamics. For example, *Nakamura et al.* [1997] first time filtered the
746 SST anomalies over the Pacific and then computed the first two EOFs for time scales
747 greater than 7 years. The first EOF shows strong variability along 40°-45°N in the west-
748 central Pacific along the subarctic front and little signal in the tropics, while the second
749 EOF has a strong loading in the tropical Pacific and along the subtropical front in the
750 central North Pacific. The first three rotated EOFs (where the patterns are no longer
751 required to be orthogonal, e.g. see *Richman*, 1986; von *Storch and Zweirs*, 1999] on
752 unfiltered monthly SST anomalies over the Pacific basin are associated with ENSO, the
753 PDO and a North Pacific mode that exhibits pronounced decadal variability (Figure 17,
754 *Barlow et al.*, 2001). The latter is similar to the leading pattern of variability identified by
755 *Nakamura et al.* [1997], although its maximum amplitude is located further east. In
756 addition, variables such as salinity, thermocline depth, and SSH may provide a more

757 direct estimate of dynamically driven ocean variability. *Di Lorenzo et al.* [2007] recently
758 identified the North Pacific Gyre Oscillation (NPGO) as the dominant mode of SSH
759 variability that has a dipole structure associated with out-of-phase changes in strength of
760 the subtropical and subpolar gyres in the eastern half of the basin. The NPGO also
761 exhibits decadal variability. The mechanism(s) behind these extratropical decadal
762 variations and the extent to which they are influenced by global warming requires further
763 study.

764 Many of the processes that operate in the North Pacific are also found in the North
765 Atlantic and the Southern Oceans where they influence the large-scale SST anomaly
766 patterns. Heat flux forcing associated with fluctuations in the North Atlantic Oscillation
767 (NAO, with opposing SLP anomaly centers over the subtropics and Icelandic) create an
768 SST tripole pattern with anomalies of one sign in midlatitudes, flanked by anomalies of
769 the opposite sign in the subtropics and subpolar regions [e.g., *Cayan*, 1992b; *Seager et*
770 *al.*, 2000]. Oceanic Rossby waves, gyre adjustments and wind driven currents also play
771 an important role in decadal variability of the Gulf Stream [e.g. *Frankignoul et al.*, 1997;
772 *Curry and McCartney*, 2004; *de Coëtlogon et al.*, 2006], although the direct connection
773 between Rossby waves and the Gulf Stream is less apparent than in the KE region. The
774 atmospheric bridge also influences the North Atlantic particularly in the subtropics, while
775 there is also a NAO-like response in mid and high latitudes that is stronger during La
776 Niña than El Niño events [e.g. *Pozo-Vázquez et al*., 2001; *Alexander et al*., 2002;
777 *Alexander and Scott*, 2008]. Modeling studies also indicate that the atmospheric response
778 to tropical Atlantic SST anomalies influences air-sea interaction and SST variability in
779 the North Atlantic [*Drevillon et al.*, 2003; Peng et al., 2005, 2006]. In the Southern

780 Hemisphere, the Southern Annular mode (SAM, with nearly zonally symmetric SLP
781 anomalies with opposing centers between 30°S-50°S and 50°-90°S), and ENSO
782 teleconnections drive SST anomalies in mid and high latitudes [*Ciasto and Thompson*,
783 2008]. In contrast to the Pacific, the meridional overturning circulation (MOC) and
784 interactions with sea ice, have a much greater impact on low-frequency SST variability in
785 the North Atlantic and parts of the Southern Ocean compared to the North Pacific.
786
787 Acknowledgements
788 I thank James Scott for preparing many of the figures and Clara Deser and an
789 anonymous reviewer for their insightful comments. The work presented here was
790 supported by grants from the NOAA Office of Global Programs and the NSF Climate
791 large-scale Dynamics program.
792
793 References
794 Alexander, M. A. (1990), Simulation of the response of the North Pacific Ocean to the
795 anomalous atmospheric circulation associated with El Niño, *Climate Dyn.*, *5*, 53-65.

796 Alexander, M. A. (1992a), Midlatitude atmosphere-ocean interaction during El Niño. Part I: the
797 North Pacific Ocean, *J. Climate*, *5*, 944-958.

798 Alexander, M. A. (1992b), Midlatitude atmosphere-ocean interaction during El Niño. Part II: the
799 north hemisphere atmosphere, *J. Climate*, *5*, 959-972.

800 Alexander, M. A., and C. Deser (1995), A mechanism for the recurrence of wintertime
801 midlatitude SST anomalies, *J. Phys. Oceanogr.*, *25*, 122-137.

802 Alexander, M. A., and C. Penland (1996), Variability in a mixed layer model driven by
803 stochastic atmospheric forcing, *J. Climate*, *9*, 2424-2442.

804 Alexander, M. A., and J. D. Scott (1997), Surface flux variability over the North Pacific and
805 North Atlantic Oceans, *J. Climate*, *10*, 2963-2978.

806 Alexander, M. A., and J. D. Scott (2008), The role of Ekman ocean heat transport in the Northern

807 Hemisphere response to ENSO, *J. Climate*, **21**, 5688-5707.

808 Alexander, M. A., C. Deser, and M. S. Timlin (1999), The re-emergence of SST anomalies in the
809 North Pacific Ocean, *J. Climate*, *12*, 2419-2433.

810 Alexander, M. A., J. D. Scott, and C. Deser (2000), Processes that influence sea surface
811 temperature and ocean mixed layer depth variability in a coupled model, *J. Geophys. Res.*,
812 *105*, 16,823-816,842.

813 Alexander, M. A., M. S. Timlin, and J. D. Scott (2001), Winter-to-Winter recurrence of sea
814 surface temperature, salinity and mixed layer depth anomalies, *Prog. Oceanogr.*, *49*, 41-61.

815 Alexander, M. A., I. Bladé, M. Newman, J. R. Lanzante, N.-C. Lau, and J. D. Scott, (2002), The
816 atmospheric bridge: the influence of ENSO teleconnections on air-sea interaction over the
817 global oceans, *J. Climate*, *15***,** 2205-2231.

818 Alexander, M. A., N.-C. Lau, and J. D. Scott (2004), Broadening the atmospheric bridge
819 paradigm: ENSO teleconnections to the North Pacific in summer and to the tropical west
820 Pacific-Indian oceans over the seasonal cycle, in *Earth's Climate: The Ocean- Atmosphere*
821 *Interaction*, edited by C. Wang, S.-P. Xie, and J. A. Carton, pp. 85-104, AGU, Washington,
822 D. C. .

823 Alexander, M. A., L. Matrosova, C. Penland, J. D. Scott, and P. Chang (2008), Forecasting
824 Pacific SSTs: Linear Inverse Model Predictions of the PDO, *J. Climate*, *21*, 385-402.

825 Barlow, M., S. Nigam, and E. H. Berbery (2001), ENSO, Pacific Decadal Variability, and U.S.
826 Summertime Precipitation, Drought, and Stream Flow, *J. Climate*, *14*, 2105–2128.

827 Barnett, T., D. W. Pierce, M. Latif, D. Dommonget, and R. Saravanan (1999), Interdecadal
828 interactions between the tropics and the midlatitudes in the Pacific basin, *Geophys. Res. Lett.*,
829 *26*, 615-618.

830 Barsugli, J. J., and D. S. Battisti (1998), The basic effects of atmosphere-ocean thermal coupling
831 on midlatitude variability, *J. Atmos. Sci.*, *55*, 477-493.

832 Benson, A. J., and A. W. Trites (2002), Ecological effects of regime shifts in the Bering Sea and
833 eastern North Pacific Ocean, *Fish and Fisheries*, *3*, 95-113.

834 Bhatt, U. S., M. A. Alexander, D. S. Battisti, D. D. Houghton, and L. M. Keller (1998),
835 Atmosphere-ocean interaction in the North Atlantic: near-surface climate variability, *J.*
836 *Climate*, *11*, 1615-1632.

837 Biondi, F., A. Gershunov, and D. R. Cayan (2001), North Pacific decadal climate variability
838 since 1661, *J. Climate*, *14*, 5–10.

839 Bjerknes, J. (1964), Atlantic air-sea interaction, *Adv. in Geophys*, *20*, 1-82.

840 Bladé, I. (1997), The influence of midlatitude coupling on the low frequency variability of a

841 GCM. Part I: No tropical SST forcing, *J. Climate*, *10*, 2087-2106.

842 Bladé, I. (1999), The influence of midlatitude ocean-atmosphere coupling on the low-frequency
843 variability of a GCM. Part II: Interannual variability induced by tropical SST forcing, *J.*
844 *Climate*, *12*, 21-45.

845 Capotondi, A., M. A. Alexander, and C. Deser (2003), Why are there Rossby wave maxima at
846 10°S and 13°N in the Pacific?, *J. Phys. Oceanogr.*, *33*, 1549-1563.

847 Capotondi, Antonietta, Michael A. Alexander, Clara Deser, and M. McPhaden (2005) Anatomy
848 and Decadal Evolution of the Pacific Subtropical Cells. *J. Climate*, *18*, 3739-3758.

849 Carton, J. A., and B. S. Giese (2008), A reanalysis of ocean climate using Simple Ocean Data
850 Assimilation (SODA), *Mon. Wea. Rev.*, *136*, 2999-3017

851 Cayan, D. R. (1992a), Variability of latent and sensible heat fluxes estimated using bulk
852 formulae, *Atmos.-Ocean*, *30*, 1-42.

853 Cayan, D. R. (1992b), Latent and sensible heat flux anomalies over the northern oceans: the
854 connection to monthly atmospheric circulation, *J. Climate*, *5*, 354-369.

855 Cayan, D. R. (1992c), Latent and sensible heat flux anomalies over the northern oceans: driving
856 the sea surface temperature, *J. Phys. Oceanogr.*, *22*, 859-881.

857 Chelton, D. B., and R. E. Davis (1982), Monthly mean sea level variability along the west coast
858 of North America, *J. Phys. Oceanogr.*, *15*, 2446 – 2461.

859 Chelton, D. B., and M. G. Schlax (1996), Global observations of oceanic Rossby waves, *Science*,
860 *272*, 234-238.

861 Ciasto, L.M., and D.W.J. Thompson, (2008), Observations of Large-Scale Ocean–
862 Atmosphere Interaction in the Southern Hemisphere, *J. Climate*, **21**, 1244–1259.
863
864 Clarke, A. J., and S. van Gorder (1994), On ENSO coastal currents and sea levels, *J. Phys.*
865 *Oceanog.*, *24*, 661–680.

866 Curry R. G., and M. McCartney, (2001), Ocean gyre circulation changes associated with the
867 North Atlantic Oscillation, *J. Phys. Oceanogr.*, **31**, 3374–3400.

868 Czaja, A. (2003), On the time variability of the net ocean to atmosphere heat flux in midlatitudes,
869 with application to the North Atlantic basin, *Quart. J. Roy. Met. Soc.*, *129*, 2867-2878.

870 Dawe, J. T., and L. Thompson (2007), PDO-related heat and temperature budget changes in a
871 model of the North Pacific, *J. Climate*, *20*, 2092–2108.

872 de Coëtlogon, G., and C. Frankignoul (2003), On the persistence of winter sea surface
873 temperature in the North Atlantic, *J. Climate*, *16*, 1364–1377.

de Coëtlogon, G., C. Frankignoul, M. Bentsen, C. Delon, H. Haak, S. Massina, and A. Pardaens, (2006), Gulf Stream variability in five oceanic general circulation models, *J. Phys. Oceanogr.,* **36**, 2119-2135.

Deser, C., and A. S. Phillips, (2006), Simulation of the 1976/1977 Climate Transition over the North Pacific: Sensitivity to Tropical Forcing, *J. Climate, 19*, 6170-6180.

Deser, C., M. A. Alexander, and M. S. Timlin (1996), Upper ocean thermal variations in the North Pacific during 1970 - 1991, *J. Climate*, *9*, 1841-1855.

Deser, C., M. A. Alexander, and M. S. Timlin (1999), Evidence for wind-driven intensification of the Kuroshio Current Extension from the 1970s to the 1980s, *J. Climate*, *12*, 1697-1706.

Deser, C., M. A. Alexander, and M. S. Timlin (2003), Understanding the persistence of sea surface temperature anomalies in midlatitudes, *J. Climate*, *16*(1), 57-72.

Deser, C., A. S. Phillips, and J. W. Hurrell (2004), Pacific interdecadal climate variability: Linkages between the Tropics and the North Pacific during boreal winter since 1900, *J. Climate*, *17*, 3109–3124.

Di Lorenzo, E., et al. (2008), North Pacific Gyre Oscillation links ocean climate and ecosystem change., *Geophys. Res. Lett.*, *35*(L08607), doi:10.1029/2007GL032838. .

Dickinson, R. E. (1978), Rossby waves - long period oscillations of oceans and atmospheres, *Annu. Rev. Fluid Mech.*, *10*, 159-195.

Dommenget, D., and M. Latif (2002), Analysis of observed and simulated spectra in the midlatitudes, *Climate Dyn.*, *19*(277-288).

Drevillon, M., C. Cassou, and L. Terray (2003), Model study of the North Atlantic region atmospheric response to autumn tropical Atlantic sea-surface-temperature anomalies. *Quart. J. Roy. Meteor. Soc.*, **129,** 2591-2611.

Elsberry, R., and R. W. Garwood (1978), Sea surface temperature anomaly generation in relation to atmospheric storms, *Bull. Amer. Meteor. Soc.*, *59*, 786-789.

Enfield, D. B., and J. S. Allen (1980), On the structure and dynamics of monthly mean sea level anomalies along the Pacific coast of North and South America, *J. Phys. Oceanogr.*, *10*, 557-588.

Fine, R. A., J. L. Reid, and H. G. Östlund (1981), Circulation of tritium in the Pacific Ocean, *J. Phys. Oceanogr.*, *11*, 3-14.

Fine, R. A., W. H. Peterson, C. G. Rooth, and H. G. Östlund (1983), Cross-equatorial tracer transport in the upper waters of the Pacific Ocean, *J. Geophys. Res.*, *88*(C1), 763-769.

Folland, C. K., J. A. Renwick, M. J. Salinger, and A. B. Mullan (2002), Relative influences of the Interdecadal Pacific Oscillation and ENSO on the South Pacific convergence zone, *Geophys. Res. Lett.*, *29*(1643), doi:10.1029/2001GL014201.

909 Frankignoul, C. (1985), Sea surface temperature anomalies, planetary waves, and air-sea
910 feedback in the middle latitudes, *Rev. Geophys.*, *23*, 357-390.

911 Frankignoul, C., and K. Hasselmann (1977), Stochastic climate models. Part 2. Application to
912 sea-surface temperature variability and thermocline variability, *Tellus*, *29*, 284-305.

913 Frankignoul, C., and E. Kestenare (2002), The surface heat flux feedback. Part I: Estimates from
914 observations in the Atlantic and the North Pacific, *Climate Dyn.*, *19*, 633-647.

915 Frankignoul, C., and R. W. Reynolds (1983), Testing a dynamical model for mid-latitude sea
916 surface temperature anomalies, *J. Phys. Oceanogr.*, *13*, 1131-1145.

917 Frankignoul, C., and N. Sennéchael (2007), Observed influence of North Pacific SST anomalies
918 on the atmospheric circulation, *J. Climate*, *20*, 592–606.

919 Frankignoul, C., P. Müller, and E. Zorita (1997), A simple model of the decadal response of the
920 ocean to stochastic wind forcing, *J. Phys. Oceanogr.*, *27*, 1533-1546.

921 Fu, L.-L., and B. Qiu (2002), Low-frequency variability of the North Pacific Ocean: the roles of
922 boundary-driven and wind-driven baroclinic Rossby waves. *J. Geophys. Res.*, *107*,
923 doi:10.1029/2001JC001131.

924 Garreaud, R. D., and D. S. Battisti (1999), Interannual (ENSO) and Interdecadal (ENSO-like)
925 variability in the southern hemisphere tropospheric circulation, *J. Climate*, *12*, 2113-2123.

926 Gedalof, Z., N. J. Mantua, and D. L. Peterson (2002), A multi-century perspective of variability
927 in the Pacific Decadal Oscillation: New insights from tree rings and coral, *Geophys. Res.*
928 *Lett.*, *29*(2204), doi:10.1029/2002GL015824.

929 Gill, A. E. (1982), *Atmosphere-Ocean Dynamics*, 662 pp., Academic Press, New York.

930 Graham, N. E., et al. (1994), On the roles of Tropical and mid-latitude SSTs in forcing
931 interannual to interdecadal variability in the winter northern hemisphere circulation, *J.*
932 *Climate*, *7*(9), 1416-1441.

933 Gu, D., and S. G. H. Philander (1997), Interdecadal climate fluctuations that depend on
934 exchanges between the tropics and extratropics, *Science*, *275*, 805-807.

935 Hanawa, K., and S. Sugimoto (2004), 'Reemergence' areas of winter sea surface temperature
936 anomalies in the world's oceans, Geophys. Res. Lett., *31*, doi:10.1029/2004GL019904.

937 Hasselmann, K. (1976), Stochastic climate models, *Tellus*, *28*, 473-485.

938 Huang, R. X., and B. Qiu (1994), Three-dimensional structure of the wind-driven circulation in
939 the subtropical North Pacific, *J. Phys. Oceanogr.*, *24*, 1608-1622.

940 Iwasaka, N., and J. M. Wallace (1995), Large scale air sea interaction in the Northern
941 Hemisphere from a view point of variations of surface heat flux by SVD analysis, *J. Meteor.*

942 *Soc. Japan*, *73*, 781-794.

943 Jacobs, G. A., H. E. Hurlburt, J. C. Kindle, E. J. Metzger, J. L. Mitchell, and A. J. Wallcraft
944 (1994), Decade-scale trans-Pacific propagation and warming effects of an El Niño anomaly,
945 *Nature*, *370***,** 360-363.

946 Ji, M., A. Leetmaa, and J. Derber (1995), An ocean analyses system for seasonal to
947 interannual climate studies, *Mon. Wea. Rev.*, *123*, 460-480.
948
949 Jin, F. F. (1997), A theory for interdecadal climate variability of the North Pacific ocean-
950 atmosphere system, *J. Climate*, *10*, 1821-1835.

951 Johnson, G. C., M. J. McPhaden, and E. Firing. (2001), Equatorial Pacific Ocean horizontal
952 velocity, divergence, and upwelling, *J. Phys. Oceanogr.*, *31*, 839-849.

953 Kalnay, E., and Coauthors (1996), The NCEP/NCAR 40-year reanalysis project., *Bull. Amer.*
954 *Meteor. Soc.*, *77*, 437-471.

955 Kelly, K. A. (2004), The relationship between oceanic heat transport and surface fluxes in the
956 western North Pacific: 1970– 2000, *J. Climate*, *17*, 573-588.

957 Kistler, R., et al. (2001), The NCEP-NCAR 50-year reanalysis: Monthly Means CD-ROM and
958 documentation, *Bull. Amer. Met. Soc.*, *82*, 247-267.

959 Kleeman, R., J. P. McCreary, and B. A. Klinger (1999), A mechanism for the decadal variation
960 of ENSO, *Geophys. Res. Lett.*, *26*, 1743 – 1747.

961 Klein, S. A., D. L. Hartmann, and J. R. Norris (1995), On the relationships among low-cloud
962 structure, sea surface temperature and atmospheric circulation in the summertime northeast
963 Pacific, *J. Climate*, *8*, 1140-1155.

964 Klein, S. A., B. J. Soden, and N.-C. Lau (1999), Remote sea surface variations during ENSO:
965 evidence for a tropical atmospheric bridge, *J. Climate*, *12*, 917-932.

966 Kushnir, Y., W. A. Robinson, I. Bladé, N. M. J. Hall, S. Peng, and R. Sutton (2002),
967 Atmospheric response to extratropical SST anomalies: Synthesis and evaluation, *J. Climate*,
968 *15*, 2205-2231.
969
970 Kwon, Y. O., and C. Deser (2007), North Pacific decadal variability in the Community Climate
971 System Model Version 2, *J. Climate*, *20*, 2416-2433.

972 Latif, M., and T. P. Barnett (1994), Causes of decadal climate variability over the North Pacific
973 and North America, *Science*, *266*, 634-637.

974 Latif, M., and T. P. Barnett (1996), Decadal climate variability over the North Pacific and North
975 America: dynamics and predictability, *J. Climate*, *9*, 2407-2423.

976 Lau, N. C., and M. J. Nath (1994), A modeling study of the relative roles of tropical and

977 extratropical SST anomalies in the variability of the global atmosphere-ocean system, *J.*
978 *Climate*, *7*, 1184-1207.

979 Lau, N.-C., and M. J. Nath (1996), The role of the 'atmospheric bridge' in linking tropical Pacific
980 ENSO events to extratropical SST anomalies., *J. Climate*, *9*, 2036-2057.

981 Lau, N.-C., and M. J. Nath (2001), Impact of ENSO on SST variability in the North Pacific and
982 North Atlantic: seasonal dependence and role of extratropical air-sea coupling., *J. Climate*,
983 *14*, 2846-2866.

984 Lee, D. E., Z. Liu, and Y. Liu (2008), Beyond thermal interaction between ocean and
985 atmosphere: On the extratropical climate variability due to the wind-induced SST, *J. Climate*,
986 *21*, 2001–2018

987 Liu, Z. (1994), A simple model of the mass exchange between the subtropical and tropical ocean,
988 *J. Phys. Oceanogr.*, *24*, 1153-1165.

989 Liu, Z., and M. A. Alexander (2007), Atmospheric Bridge, Oceanic Tunnel and Global Climatic
990 Teleconnections, *Rev. Geophys.*, *45*, RG2005, doi:2010.1029/2005RG000172.

991 Liu, Z., and L. Wu (2004), Atmospheric Response to North Pacific SST: The role of ocean-
992 atmosphere coupling, *J. Climate*, *17*, 1859-1882.

993 Liu, Z., L. Wu, R. Gallimore, and R. Jacob (2002), Search for the Origins of Pacific Decadal
994 Climate Variability, *Geophysical Research Letters*, *29*(10), doi:1029/2001GL013735.

995 Luo, J. J., and T. Yamagata (2001), Long-term El Niño – Southern Oscillation (ENSO)-like
996 variation with special emphasis on the South Pacific, *J. Geophys. Res.*, *106*, 22,211 –
997 222,227.

998 Mantua, N. J., S. R. Hare, Y. Zhang, J. M. Wallace, and R. Francis (1997), A Pacific
999 interdecadal climate oscillation with impacts on salmon production, *Bull. Amer.*
1000 *Meteor. Soc.*, *78*(6), 1069-1079.
1001
1002 McCreary, J. P., and P. Lu (1994), Interaction between the subtropical and equatorial ocean
1003 circulations: the subtropical cell, *J. Phys. Oceanogr.*, *24*, 466-497.

1004 McPhaden, M. J., and D. Zhang (2002), Slowdown of the meridional overturning circulation in
1005 the upper Pacific Ocean, *Nature*, *415*, 603 – 608.

1006 Mestas-Nuñez, A. M., and D. B. Enfield (1999), Rotated global modes of non-ENSO sea surface
1007 temperature variability, *J. Climate*, *12*, 2734–2746.

1008 Meyers, S. D., M. A. Johnson, M. Liu, J. J. O'brien, and J. L. Spiesberger (1996),
1009 Interdecadal variability in a numerical model of the northeast Pacific: 1970-89, *J.*
1010 *Phys. Oceanogr.*, *26*, 2635-2652.
1011
1012 Miller, A. J. and N. Schneider (2000), Interdecadal climate regime dynamics in the North

1013 Pacific Ocean: theories, observations, and ecosystem impacts. *Prog. Oceanogr.*, *47***,** 355-
1014 379.
1015
1016 Miller, A. J., D. R. Cayan, T. P. Barnett, N. E. Graham, and J. M. Oberhuber (1994),
1017 Interdecadal variability of the Pacific Ocean: model response to observed heat flux
1018 and wind stress anomalies, *Climate Dyn.*, *10*, 287-302.
1019
1020 Miller, A. J., W. B. White, and D. R. Cayan (1997), North Pacific thermocline variations
1021 on ENSO timescales, *J. Phys. Oceanogr.*, *27*, 2023-2039.
1022
1023 Monterey, G. I., and S. Levitus (1997), *Climatological Cycle of Mixed Layer Depth in the World*
1024 *Ocean*, 5 pp., 87 figs. pp., U.S. Gov. Printing Office, NOAA NESDIS, Wash., D.C.

1025 Nakamura, H., H. G. Lin, and T. Yamagata (1997), Decadal climate variability in the North
1026 Pacific in recent decades, *Bull. Amer. Met.Soc.*, *78*, 2215-2226.

1027 Namias, J. (1959), Recent seasonal interactions between North Pacific waters and the overlying
1028 atmospheric circulation, *J. Geophys. Res.*, *64*, 631-646.

1029 Namias, J. (1963), Large-scale air-sea interactions over the North Pacific from summer (1962)
1030 through the subsequent winter, *J. Geophys. Res.*, *68*, 6171-6186.

1031 Namais, J. (1965), Macroscopic association between mean monthly sea surface temperature and
1032 the overlying winds, *J. Geophys. Res.*, *70*, 2307-2318.

1033 Namias, J. (1969), Seasonal interactions between the North Pacific Ocean and the atmosphere
1034 during the 1960's, *Mon. Wea. Rev.*, *97*, 173-192.

1035 Namias, J., and R. M. Born (1970), Temporal coherence in North Pacific sea-surface temperature
1036 patterns, *J. Geophys. Res.*, *75*, 5952-5955.

1037 Namias, J., and R. M. Born (1974), Further studies of temporal coherence in North Pacific sea
1038 surface temperatures, *J. Geophys. Res.*, *79*, 797-798.

1039 Neelin, J. D., D. S. Battisti, A. C. Hirst, F. F. Jin, Y. Wakata, T. Yamagata and S. Zebiak, (1998),
1040 ENSO theory, *J. Geophys. Res.*, *103***,** 14,261-14,290.

1041 Newman, M. (2007), Interannual to decadal predictability of tropical and North Pacific sea
1042 surface temperatures, *J. Climate*, *20*, 2333-2356.

1043 Newman, M., G. Compo, and M. A. Alexander (2003), ENSO-forced variability of the Pacific
1044 Decadal Oscillation, *J. Climate*, *16*, 3853-3857.

1045 Norris, J. R., and C. Leovy (1994), Interannual variability in stratiform cloudiness and sea
1046 surface temperature, *J. Climate*, *7*, 1915-1925.

1047 Norris, J. R., Y. Zhang, and J. M. Wallace (1998), Role of clouds in summertime
1048 atmosphere-ocean interactions over the North Pacific, *J. Climate*, *11*, 2482-2490.

Ortiz, M. J., and A. Ruiz de Elvia (1985), A cyclo-stationary model of sea surface temperature in the Pacific Ocean, *Tellus*, *37A*, 14-23.

Park, S., and C. B. Leovy (2004), Marine low-cloud anomalies associated with ENSO, *J. Climate*, *17*, 3448 – 3469.

Park, S., C. Deser, and M. A. Alexander (2005), Estimation of the surface heat flux response to sea surface temperature anomalies over the global oceans. *J. Climate*, *18*, 4582–4599.

Park, S., M. A. Alexander and C. Deser (2006), The impact of cloud radiative feedback, remote ENSO forcing, and entrainment on the persistence of North Pacific sea surface temperature anomalies, *J. Climate*, *19*, 6243-6261.

Peng, S., W. A. Robinson, and M. P. Hoerling (1997), The modeled atmospheric response to midlatitude SST anomalies and its dependence on background circulation states, *J. Climate*, *10*, 971-987.

Peng, S., and J. S. Whitaker (1999), Mechanisms determining the atmospheric response to midlatitude SST anomalies, *J. Climate*, *12*, 1393-1408.

Peng, S., W. A. Robinson, S. Li, and M. P. Hoerling, (2005), Tropical Atlantic SST forcing of coupled North Atlantic seasonal responses, *J. Climate*, **18,** 480-496.

Peng, S., W.A. Robinson, S. Li, and M.A. Alexander, (2006), Effects of Ekman transport on the NAO response to a tropical Atlantic SST anomaly, *J. Climate*, **19,** 4803-4818.

Pierce, D. W. (2001), Distinguishing coupled ocean-atmosphere interactions from background noise in the North Pacific, *Prog. Oceanogr.*, *49*, 331-352.

Pierce, D. W., T. P. Barnett, and M. Latif (2000), Connections between the Pacific Ocean tropics and midlatitudes on decadal timescales, *J. Climate*, *13*, 1173-1194.

Power, S. B., T. Casey, C. Folland, A. Colman, and V. Mehta (1999), Interdecadal modulation of the impact of ENSO on Australia, *Climate Dyn.*, *15*, 319–324.

Pozo-Vázquez, D., M. J. Esteban-Parra, F. S. Rodrigo, and Y. Castro-Díez (2001), The association between ENSO and winter atmospheric circulation and temperature in the North Atlantic region. *J. Climate*, **14,** 3408–3420.

Qiu, B. (2000), Interannual variability of the Kuroshio Extension system and its impact on the wintertime SST field, *J. Phys. Oceanogr.*, *30*, 1486-1502.

Qiu, B. (2003), Kuroshio Extension variability and forcing of the Pacific decadal oscillations: Responses and potential feedback, *J. Phys. Oceanog.*, *33*, 2465-2482.

Qiu, B., and S. Chen (2005), Variability of the Kuroshio Extension jet, recirculation gyre and mesoscale eddies on decadal timescales, *J. Phys. Oceanog.*, *35*, 2090-2103.

1083 Qiu, B., N. Schneider, and S. Chen (2007), Coupled decadal variability in the North Pacific: An
1084 observationally-constrained idealized model, *J. Climate*, *20*, 3602-3620.

1085 Qu, T., S.-P. Xie, H. Mitsudera, and A. Ishida (2002), Subduction of the North Pacific Mode
1086 Waters in a Global High-Resolution GCM, *J. Phys. Oceanogr.*, *32*, 746–763

1087 Rayner, N. A., P. Brohan, D. E. Parker, C .F. Folland, J. J .Kennedy, M. Vanicek, T. Ansell, and
1088 S. F. B. Tett (2006), Improved analyses of changes and uncertainties in sea surface
1089 temperature measured in situ since the mid-nineteenth century: the HadSST2 data set, *J.*
1090 *Climate*, *19*(3), 446-469.

1091 Reynolds, R. W. (1978), Sea surface temperature anomalies in the North Pacific Ocean, *Tellus*,
1092 *30*, 97-103.

1093 Reynolds, R. W., T. M. Smith, C. Liu, D. B. Chelton, K. S. Casey, and M. G. Schlax (2007),
1094 Daily high-resolution-blended analyses for sea surface temperature, *J. Climate*, *20*, 5473–
1095 5496

1096 Richman, M. B. (1986), Rotation of principal components, *6*, 293–335.

1097 Robinson, I. S. (2004), *Measuring the Oceans from Space*, 669 pp., Springer, New York.

1098 Saravanan, R. (1998), Atmospheric low frequency variability and its relationship to midlatitude
1099 SST variability: studies using the NCAR Climate System Model, *J. Climate*, *11*, 1386-1404.

1100 Saravanan, R., and J. C. McWilliams (1997), Stochasicity and spatial resonance in interdecadal
1101 climate fluctuations, *J. Climate*, *10*, 2299-2320.

1102 Saravanan, R., and J. C. McWilliams (1998), Advective ocean-atmosphere interaction: an
1103 analytical stochastic model with implications for decadal variability, *J. Climate*, *11*, 165–188.

1104 Schneider, N., and B. D. Cornuelle (2005), The forcing of the Pacific Decadal Oscillation., *J.*
1105 *Climate*, *18*, 4355-4373.

1106 Schneider, N., and A. J. Miller (2001), Predicting North Pacific Ocean climate, *J. Climate*, *14*,
1107 3997-4002.

1108 Schneider, N., A. J. Miller, M. A. Alexander, and C. Deser (1999), Subduction of decadal north
1109 Pacific temperature anomalies: observations and dynamics, *J. Phys. Oceanogr.*, *29*, 1056-
1110 1070.

1111 Schneider, N., A. J. Miller, and D. W. Pierce (2002), Anatomy of North Pacific decadal
1112 variability, *J. Climate*, *15*, 586-605.

1113 Seager R., Y. Kushnir, M. Visbeck, N. Naik, J. Miller, G. Krahmann, and H. Cullen (2000),
1114 Causes of Atlantic Ocean climate variability between 1958 and 1998. *J. Climate*, **13**, 2845–
1115 2862.

1116 Seager, R., Y. Kushnir, N. H. Naik, M. A. Cane, J. Miller (2001), Wind-driven shifts in the
1117 latitude of the Kuroshio–Oyashio Extension and generation of SST anomalies on decadal
1118 timescales, *J. Climate*, *14*, 4249–4265

1119 Smith, T. M., et al. (1996), Reconstruction of historical sea surface temperatures using empirical
1120 orthogonal functions., *J. Climate*, *9*, 1403-1420.

1121 Solomon, A., J.P. McCreary, R. Kleeman, and B.A. Klinger (2003), Interactions between
1122 interannual tropical oscillations and decadal extratropical oscillations in an intermediate
1123 coupled model of the Pacific basin, *J. Climate*, *16*, 2395-2410.

1124 Solomon, A., S.-I. Shin, M.A. Alexander, and J.P. McCreary (2008), The relative importance of
1125 tropical variability forced from the North Pacific through ocean pathways. *Climate Dyn.* , *31*,
1126 doi:10.1007/s00382-00007-00353-00387.

1127 Sugimoto, S., and K. Hanawa (2005), Remote reemergence areas of winter sea surface
1128 temperature anomalies in the North Pacific, *Geophys. Res. Lett.*, *32*.

1129 Sura, P., M. Newman, and M. A. Alexander (2006), Daily to decadal sea surface temperature
1130 variability driven by state-dependent stochastic heat fluxes, *J. Phys. Oceanogr.*, *36*, 1940-
1131 1958.

1132 Taguchi, B., S.-P. Xie, H. Mitsudera, and A. Kubokawa (2005), Response of the Kuroshio
1133 Extension to Rossby waves associated with the 1970s climate regime shift in a high-
1134 resolution ocean model. , *J. Climate*, *18*, 2979–2995.

1135 Taguchi, B., S.-P. Xie, N. Schneider, M. Nonaka, H. Sasaki, and Y. Sasai (2007), Decadal
1136 variability of the Kuroshio Extension: observations and an eddy-resolving model hindcast, *J.*
1137 *Climate*, *20*, 2357–2377

1138 Tanimoto, Y., H. Nakamura, T. Kagimoto, and S. Yamane (2003), An active role of extratropical
1139 sea surface temperature anomalies in determining anomalous turbulent heat flux, *J. Geophys.*
1140 *Res.*, *108(C10)*, doi:10.1029/2002JC001750.
1141
1142 Timlin, M. S., M. A. Alexander, and C. Deser (2002), On the reemergence of North Atlantic SST
1143 anomalies, *J. Climate*, *15*, 2707-2712.

1144 Trenberth, K. E. (1990), Recent observed interdecadal climate changes in the Northern
1145 Hemisphere, *Bull. Amer. Meteor. Soc.*, *71*, 988-993.

1146 Trenberth, K. E., G. W. Branstator, D. Karoly, A. Kumar, N-C. Lau, and C. Ropelewski (1998),
1147 Progress during TOGA in understanding and modeling global teleconnections associated
1148 with tropical sea surface temperatures, *J. Geophys. Res.*, *103*(C7), 14,291-14324.
1149
1150 Trenberth, K. E., and J. W. Hurrell (1994), Decadal atmosphere-ocean variations in the Pacific,
1151 *Climate Dyn.*, *9*, 303-319.

1152 Vimont, D. J., D. S. Battisti, and A. C. Hirst (2001), Footprinting: A seasonal link between the

1153 mid-latitudes and tropics, *Geophys. Res. Lett.*, *28*, 3923 – 3926.

1154 Vimont, D. J., J. M. Wallace, and D. S. Battisti (2003), The seasonal footprinting mechanism in
1155 the Pacific: Implications for ENSO, *J. Climate*, *16*, 2668 – 2675.

1156 von Storch, H., and F. W. Zwiers (1999), *Statistical Analysis in Climate Research* Cambridge
1157 University Press.

1158 Watanabe, M., and M. Kimoto (2000), On the persistence of decadal SST anomalies in the North
1159 Atlantic, *J. Climate*, *13*, 3017-3028.

1160 Weare, B. (1994), Interrelationships between cloud properties and SSTs on seasonal and
1161 interannual timescales., *J. Climate*, *7*, 248-260.

1162 Weng, W., and J. D. Neelin (1999), Analytical prototypes for ocean–atmosphere interaction at
1163 midlatitudes. Part II: mechanisms for coupled gyre modes, *J. Climate*, *12*, 2757–2774

1164 Wu, L., and Z. Liu (2003), Decadal Variability in the North Pacific: the Eastern North Pacific
1165 Mode, *J. Climate*, *16*, 3111-3131.

1166 Wu, L., Z. Liu, R. Gallimore, R. Jacob, D. Lee, and Y. Zhong (2003), A coupled modeling study
1167 of Pacific decadal variability: The Tropical Mode and the North Pacific Mode,, *J. Climate*,
1168 *16*, 1101 – 1120.

1169 Wu, L., D. Lee, and Z. Liu (2005), The 1976/77 North Pacific climate regime shift: the role of
1170 subtropical ocean adjustment and coupled ocean-atmosphere feedbacks, *J. Climate*, *18*, 5125-
1171 5140.

1172 Xie, S.-P., T. Kunitani, A. Kubokawa, M. Nonanka, and S. Hosoda (2000), Interdecadal
1173 thermocline variability in the North Pacific for 1958-1997: A GCM simulation, *J. Phys.*
1174 *Oceanogr*, *30*, 2798–2813

1175 Yulaeva, E., N. Schneider, D. W. Pierce, and T. Barnett (2001), Modeling of North Pacific
1176 climate variability forced by oceanic heat fluxes anomalies, *J. Climate*, *14*, 4027-4046.

1177 Zhang, Y., J. M. Wallace, and D. S. Battisti (1997), ENSO-like interdecadal variability, *J.*
1178 *Climate*, *10*(5), 1004-1020.

1179

Figure Captions

Figure 1. a) Annual mean and b) standard deviation of SST for the years 1985-2007 obtained from the NOAA high resolution (0.25° lat x lon) SST data set [*Reynolds et al.*, 2007].

Figure 2. Annual average ocean currents (m s^{-1}) averaged over the upper 500 m from the Simple Ocean Data Assimilation (SODA, *Carton and Giese*, 2008) for the years 1958-2001. The current strength is indicated by the three tone gray scale with maximum values of ~0.7 m sec^{-1} in the Kuroshio.

Figure 3. The mean ocean temperature (°C) and mixed layer depth (*h*) over the course of the seasonal cycle in a 5°x5° box centered on 50°N, 145°W (where Weathership P was located from the 1950s – 1980s) in the northeast Pacific. The temperature values are from SODA and the *h* values from *Monterey and Levitus* [1997]. Arrows denote the reemergence mechanism where surface heat flux anomalies create temperature anomalies over the deep winter mixed layer; the anomalies are then sequestered in the summer seasonal thermocline and return to the surface in the following winter.

Figure 4. The long-term mean mixed layer depth (m) during (a) Mar and (b) Sep using a density difference between the surface and base of the mixed layer of 0.125 kg m^{-3}. Data obtained from *Monterey and Levitus* [1997].

Figure 5. The Pacific subtropical cell (STC): (a) Meridional streamfunction computed from the NCAR OGCM driven by observed atmospheric surface conditions. The flow is clockwise (counter clockwise) in the Northern (Southern Hemisphere). Contour interval is 5 Sv. (b) The circulation with in the subsurface portion of the STC and subtropical gyre. Arrows indicate the averaged upper-ocean velocities, integrated from the base of the surface Ekman layer (50 m depth) to the depth of the 25 σ_θ potential density surface; contours denote the mean potential vorticity (PV) on the 25 σ_θ surface, which outcrops between 30°-40°N and the strongest equatorward flow in the subtropics. The currents tend to conserve PV, thus the large values along 10°N, act as a partial barrier, and the water subducted in the north Pacific takes a convoluted to reach the equator. Adapted from *Capotondi et al.* [2005].

Figure 6. Observed SST variance spectra (black line) in a 5°x5° box centered on 50°N, 145°W using 134 years of month anomalies from the HadSST data set [*Rayner et al.*, 2006]. The gray and white cures are based on a AR(1) model, fit to the SST data: $SST_{t+1} = r_{\tau=1} SST_t + \sigma_\varepsilon \varepsilon$, where the noise is given by $\sigma_\varepsilon = \left(\sigma\left(1 - r_{\tau=1}^2\right)\right)^2$, σ is the standard deviation and ε is a random number drawn from a Gaussian distribution. The gray shading represents the 5th and 95th percentile bounds for 1200 134-yr simulated spectra; the white line is the average of simulated spectra and overlays the theoretical spectra on an AR(1) model, the discrete form of Equation 4.

Figure 7. The reemergence mechanism as indicated by lead–lag regressions [°C (1°C)$^{-1}$] between temperature anomalies at 5 m in Apr–May, and temperature anomalies from the previous Jan through the following Apr in the (b) east, (c) central, and (d) west Pacific regions [shown in (a)]. The contour interval is 0.1 and values greater than (b) 0.55, (c) 0.7, and (d) 0.75 are shaded to highlight the reemergence mechanism. Computed using the NCEP ocean assimilation analyses [*Ji et al.*, 1995]. Adapted from *Alexander et al.* [1999].

Figure 8. Sea surface height (SSH) anomalies along the zonal band of 32°–34°N from (a) the satellite altimeter data and (b) the wind-forced baroclinic Rossby wave model; see Eq. (5). Adapted from *Qiu et al.* [2007].

Figure 9. Atmospheric a) forcing and b) response to SST anomalies in the Kuroshio extension region. Regression of wind stress curl anomalies on the winter normalized SST anomalies in the KE region (35°–45°N, 140°E–180°). (a) Annual mean wind stress curl leading SST Index by 4 yr; both variables are smoothed with a 10-yr low-pass filter. (b) Annual mean wind stress curl lagging the SST index by 1 yr based on unfiltered data. The unfiltered regression pattern is further scaled by the ratio of the standard deviation of 10-yr low-pass-filtered SST index to that of unfiltered SST index. (Contour intervals are 0.2 × 10−8 N m−3. Negative values are dashed and shading indicates regressions significant at 99%. Results are from a long coupled NCAR GCM simulation. Adapted from *Kwon and Deser* [2007].

Figure 10. Relationship between temperature anomalies in the Kuroshio Extension and changes in the ocean gyres. Simultaneous regression of DJFM subsurface zonal current velocity along 150°E on the SST anomalies averaged over the KE region. Both variables have been low-pass filtered to retain periods longer than 10 yr. Contour interval is 0.2 cm s^{-1} °C^{-1}, and the shading indicates regressions significant at 99%. Solid (dashed) contours denote eastward (westward) velocity. Thin contours with boxed labels indicate the climatological winter (DJFM) mean zonal velocity fields. Contour interval for the mean zonal velocity is 2 cm s^{-1} Results are from a long coupled NCAR GCM simulation [*Kwon and Deser,* 2007]

Figure 11. The Pacific Decadal Oscillation spatial and temporal structure: the leading pattern SST and SLP anomalies north of 20°N and normalized time series of monthly SST anomalies (PDO index, defined by Mantua et al. [1997]. Regressions of the PDO index on the (a) observed SST (ci 0.1 °C per 1σ PDO value) and (b) SLP (ci 0.25 mb per 1σ PDO value). The SSTs were obtained from the HadSST data set for the period 1900-2004, and the SLP values from NCEP Reanalysis for the years 1948-2007. (c) The monthly PDO index (gray shading) and 12-month running mean (black line) during 1900-2007, obtained from [http://jisao.washington.edu/pdo/PDO.latest].

Figure 12. The SLP, flux and SST anomaly patterns associated with the Aleutian low during winter (DJF). (a) EOF 1 of SLP, regression values of the local (b) Qnet (contour interval 2.5 W m^{-2}) and (c) SST (CI is 0.05 deg C) anomalies on PC1 of SLP, (d) EOF 1 of SST. All fields are obtained from a 50-year simulation of the GFDL AGCM coupled to an ocean MLM over the ice-free ocean.

Figure 13. Power spectrum of the observed PDO index. Dashed indicates the best fit based on a first-order autoregressive model, thin solid line shows the theoretical slope for intermediate frequency portion of the spectrum from a stochastic model. Adapted from *Qiu et al.* [2007].

Figure 14. The 1977-1988 minus the 1970-1976 average SST during NDJFM from (a) observations and (b) an ensemble average of 16 model simulations. The observations and model integrations are described in *Smith et al.* [1996] and *Alexander et al.* [2002], respectively. The model consists of an AGCM coupled to an ocean mixed layer ocean model over the ice-free global oceans except in the central/eastern tropical Pacific (box) where observed SSTs are specified. Negative values are shaded and the CI is 0.2 °C.

Figure 15. The annual a) long-term mean and b) 1977-88 minus 1986-76 wind stress (vectors) and its curl (contours) from the NCEP reanalysis. The ci is 5×10^{-8} N m^{-3} in a) and 2×10^{-8} N m^{-3} in b) where the $-1 \times 10-8$ N m−3 contour is also shown and values < $-2 \times 10-8$ N m^{-3} are shaded. The annual c) long-term mean and d) 1977-88 minus 1986-76 geostrophic transport streamfunction, given by the Sverdrup minus Ekman currents: the adjusted ocean circulation to wind curl forcing. The CI is 10 Sv in c) and 2 Sv in d), where values > 4 Sv are shaded. Adapted from Deser et al. [1999].

Figure 16. (a) The PDO time series and reconstruction (gray) based on contributions to the PDO from ENSO teleconnections (Niño-3.4*), stochastic fluctuations in the Aleutian low indicated by the North Pacific Index (NPI*), and the change in the ocean gyres given by the difference in the zonal average ocean pressure difference ($P_{DEL,}$ indicative of the slope of the thermocline and hence the strength/position of the ocean gyres) between 38° and 40°N in the KE region. The index for thermocline depth estimate from 35°-38°N in the KE region (P^*_{AVG}) does not explain a significant fraction of the SSTA variability of the PDO. Dotted vertical lines mark the winters of 1976/77 and 1998/99. (b) Power spectrum of the observed and reconstructed PDO, and contributions resulting from the NPI*, Niño34*, and P^*_{DEL}. Spectra have been smoothed by three successive applications of a five-point running mean. Note the dominance of the NPI* and ENSO* contributions to the PDO at internal annual time scales and the roughly equal contribution of the three factors at decadal time scales. From *Schenider and Cornulle* [2005].

Figure 17. The spatial patterns for the three leading modes of Pacific SST variability during 1945–93 obtained from rotated principal component analysis: (a) ENSO, (b) Pacific Decadal Oscillation, and (c) North Pacific. Adapted from *Barlow et al.* [2001].

Plate 1. The ENSO signal including the atmospheric bridge as indicated by the composite of 10 El Niño minus 10 La Niña events for SLP (contours, interval 0.5 mb) and SST (shading, interval 0.2 °C) during (a) DJF when ENSO peaks and (b) the previous JAS. The fields are obtained from NCEP atmospheric reanalysis [*Kalnay et al.*, 1996; *Kistler et al.*, 2001].

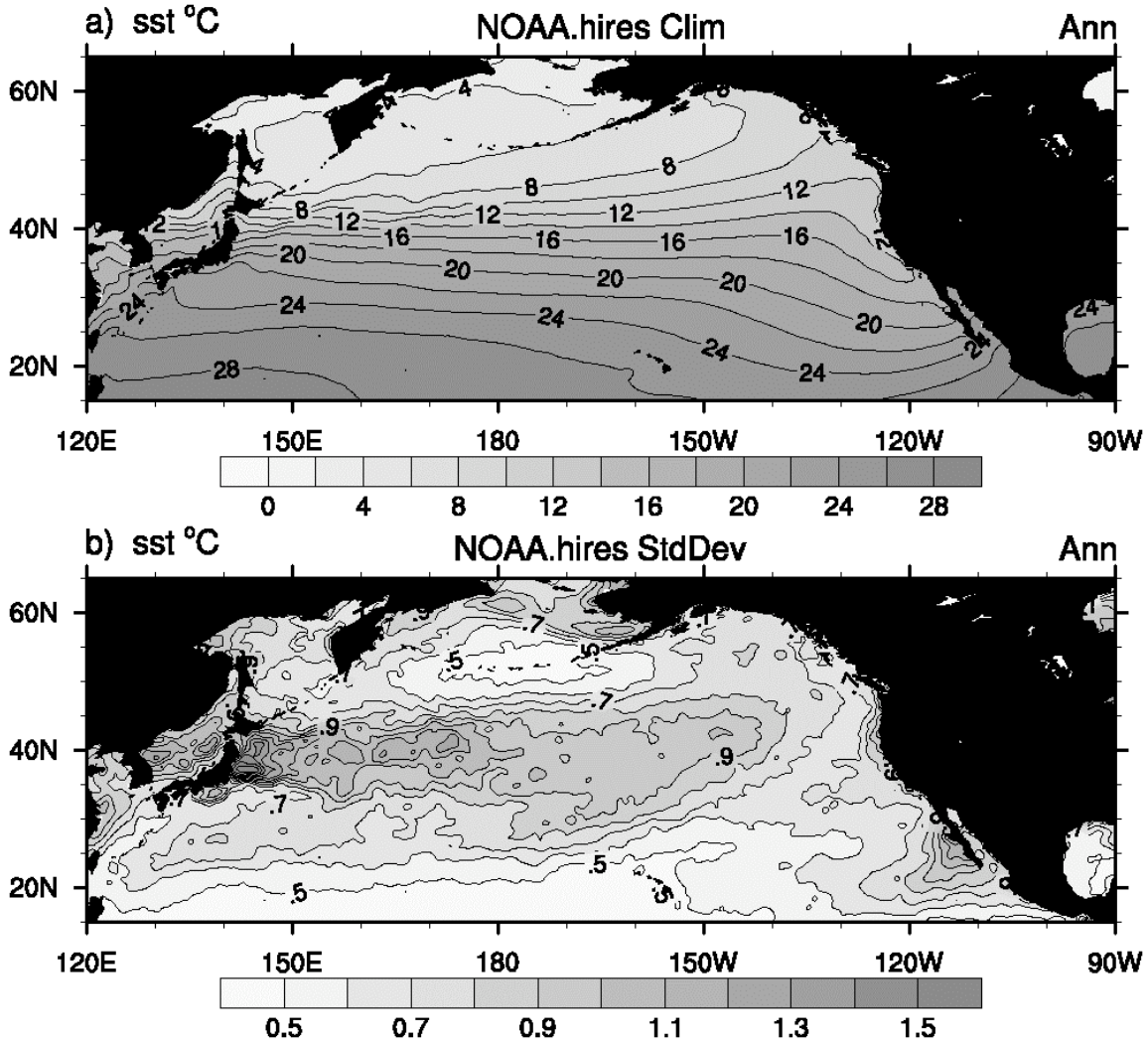

Figure 1. a) Annual mean and b) standard deviation of SST for the years 1985-2007 obtained from the NOAA high resolution (0.25° lat x lon) SST data set [*Reynolds et al.*, 2007].

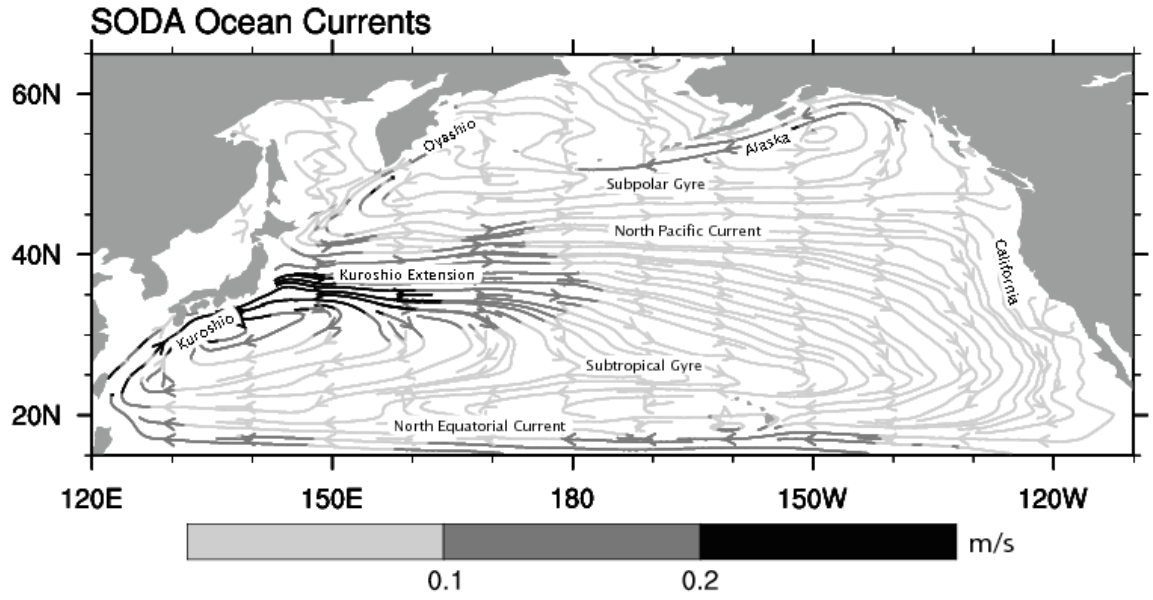

Figure 2. Annual average ocean currents (m s^{-1}) averaged over the upper 500 m from the Simple Ocean Data Assimilation (SODA, *Carton and Giese*, 2008) for the years 1958-2001. The current strength is indicated by the three tone gray scale with maximum values of ~0.7 m sec^{-1} in the Kuroshio.

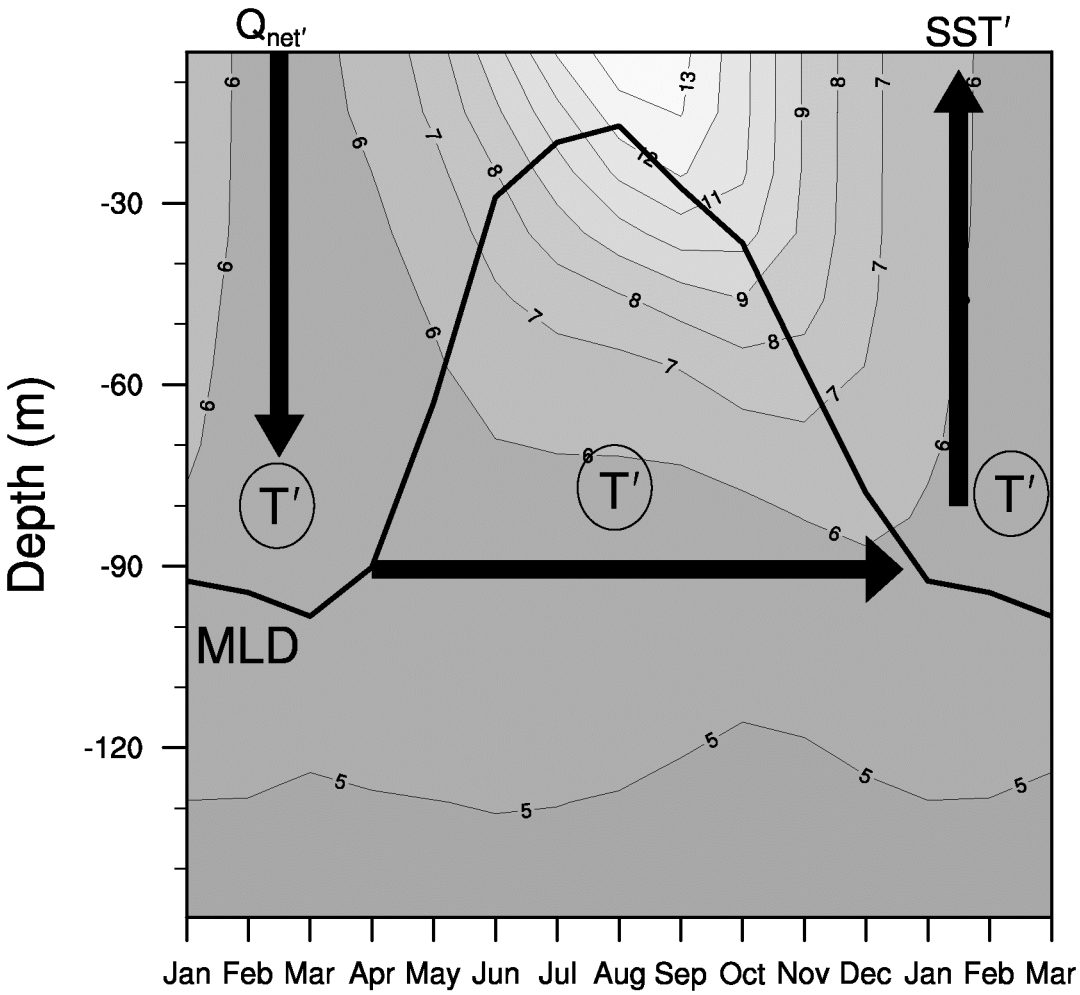

Figure 3. The mean ocean temperature (°C) and mixed layer depth (*h*) over the course of the seasonal cycle in a 5°x5° box centered on 50°N, 145°W (where Weathership P was located from the 1950s – 1980s) in the northeast Pacific. The temperature values are from SODA and the *h* values from *Monterey and Levitus* [1997]. Arrows denote the reemergence mechanism where surface heat flux anomalies create temperature anomalies over the deep winter mixed layer; the anomalies are then sequestered in the summer seasonal thermocline and return to the surface in the following winter.

1342

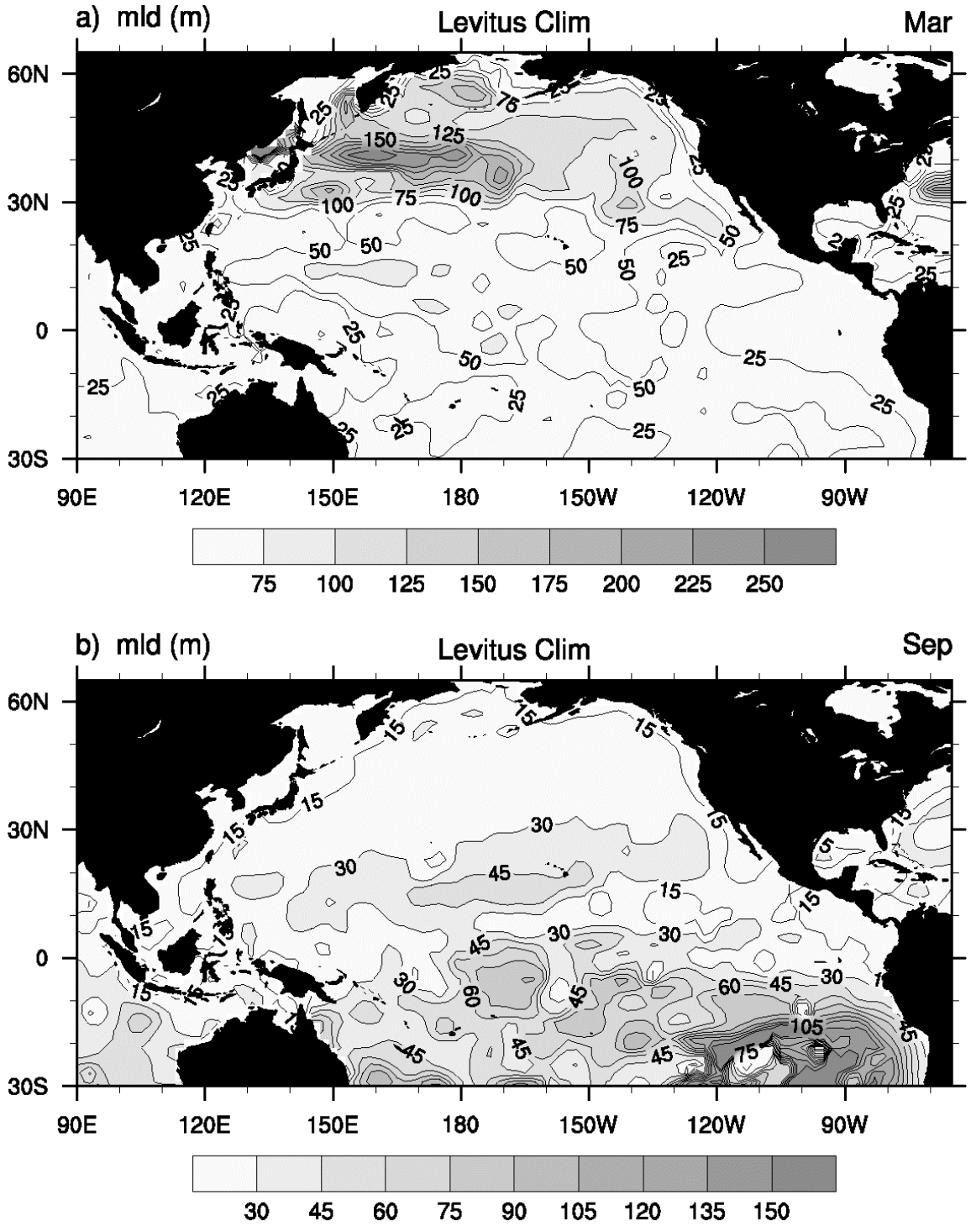

1343
1344

1345 Figure 4. The long-term mean mixed layer depth (m) during (a) Mar and (b) Sep using a
1346 density difference between the surface and base of the mixed layer of 0.125 kg m^{-3}. Data
1347 obtained from *Monterey and Levitus* [1997].
1348

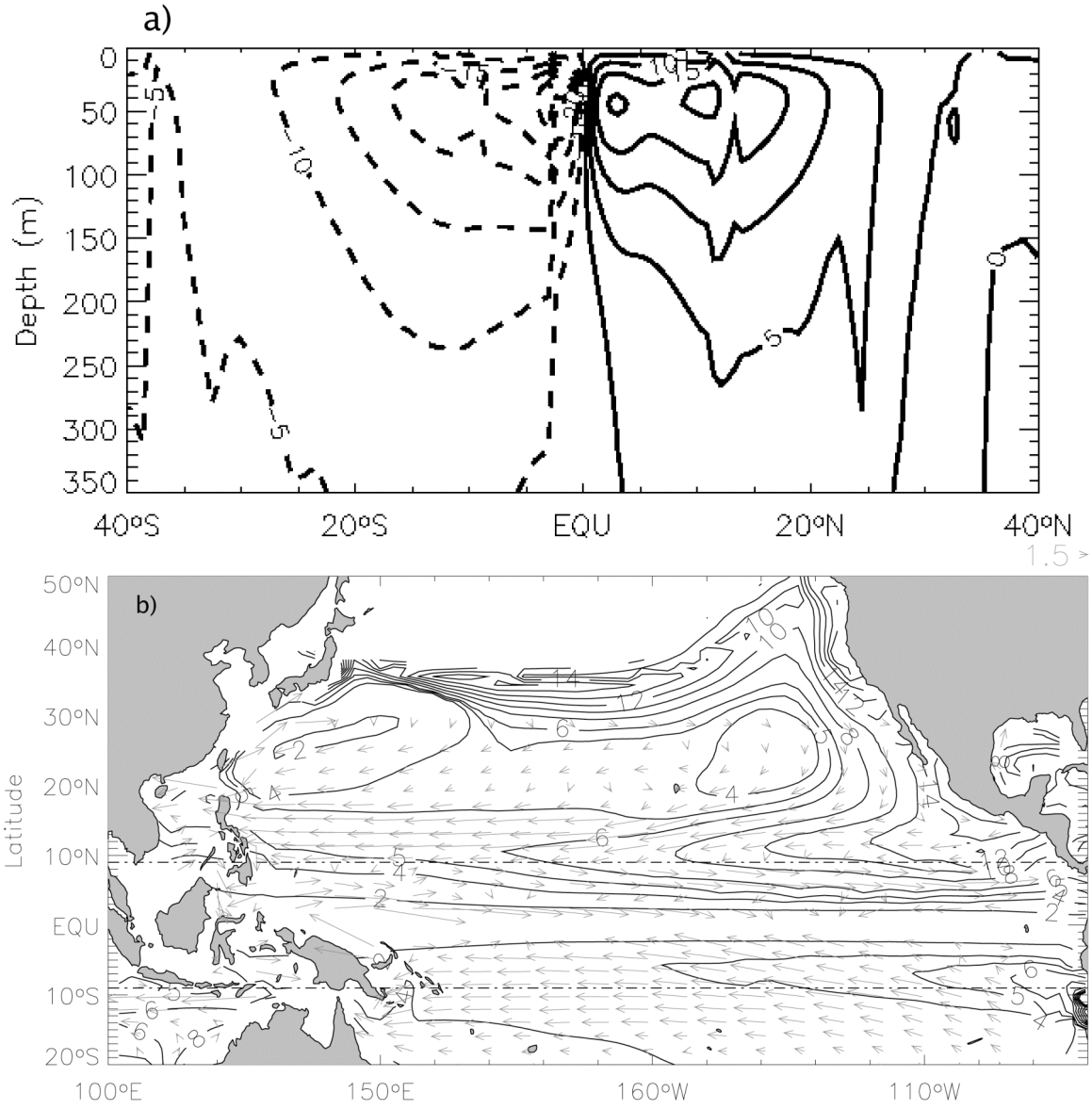

Figure 5. The Pacific subtropical cell (STC): (a) Meridional streamfunction computed from the NCAR OGCM driven by observed atmospheric surface conditions. The flow is clockwise (counter clockwise) in the Northern (Southern Hemisphere). Contour interval is 5 Sv. (b) The circulation with in the subsurface portion of the STC and subtropical gyre. Arrows indicate the averaged upper-ocean velocities, integrated from the base of the surface Ekman layer (50 m depth) to the depth of the 25 σ_θ potential density surface; contours denote the mean potential vorticity (PV) on the 25 σ_θ surface, which outcrops between 30°-40°N and the strongest equatorward flow in the subtropics. The currents tend to conserve PV, thus the large values along 10°N, act as a partial barrier, and the water subducted in the north Pacific takes a convoluted to reach the equator. Adapted from *Capotondi et al.* [2005].

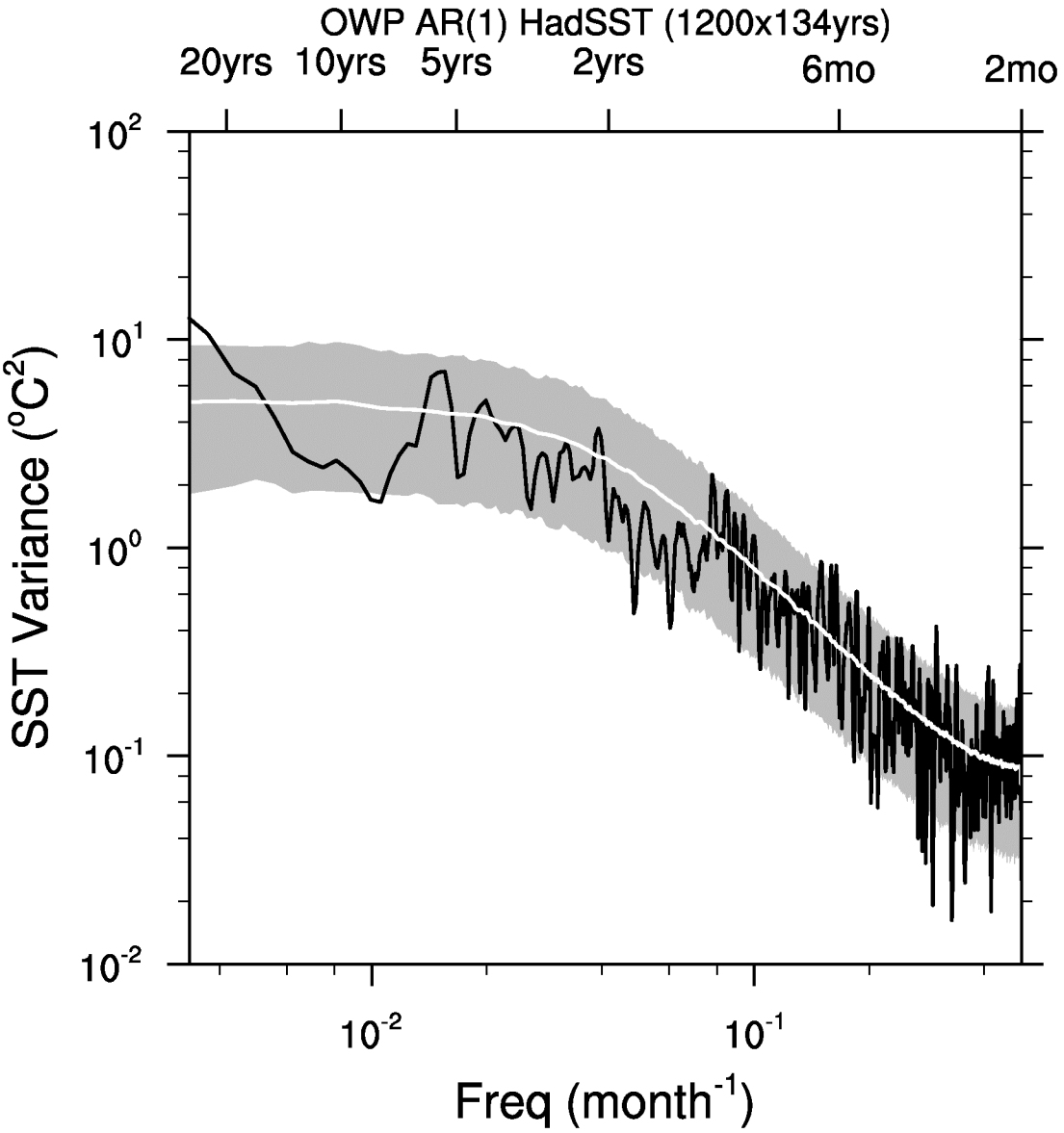

Figure 6. Observed SST variance spectra (black line) in a 5°x5° box centered on 50°N, 145°W using 134 years of month anomalies from the HadSST data set [*Rayner et al.*, 2006]. The gray and white cures are based on a AR(1) model, fit to the SST data: $SST_{t+1} = r_{\tau=1} SST_t + \sigma_\varepsilon \varepsilon$, where the noise is given by $\sigma_\varepsilon = \left(\sigma\left(1 - r_{\tau=1}^2\right)\right)^2$, σ is the standard deviation and ε is a random number drawn from a Gaussian distribution. The gray shading represents the 5th and 95th percentile bounds for 1200 134-yr simulated spectra; the white line is the average of simulated spectra and overlays the theoretical spectra on an AR(1) model, the discrete form of Equation 4.

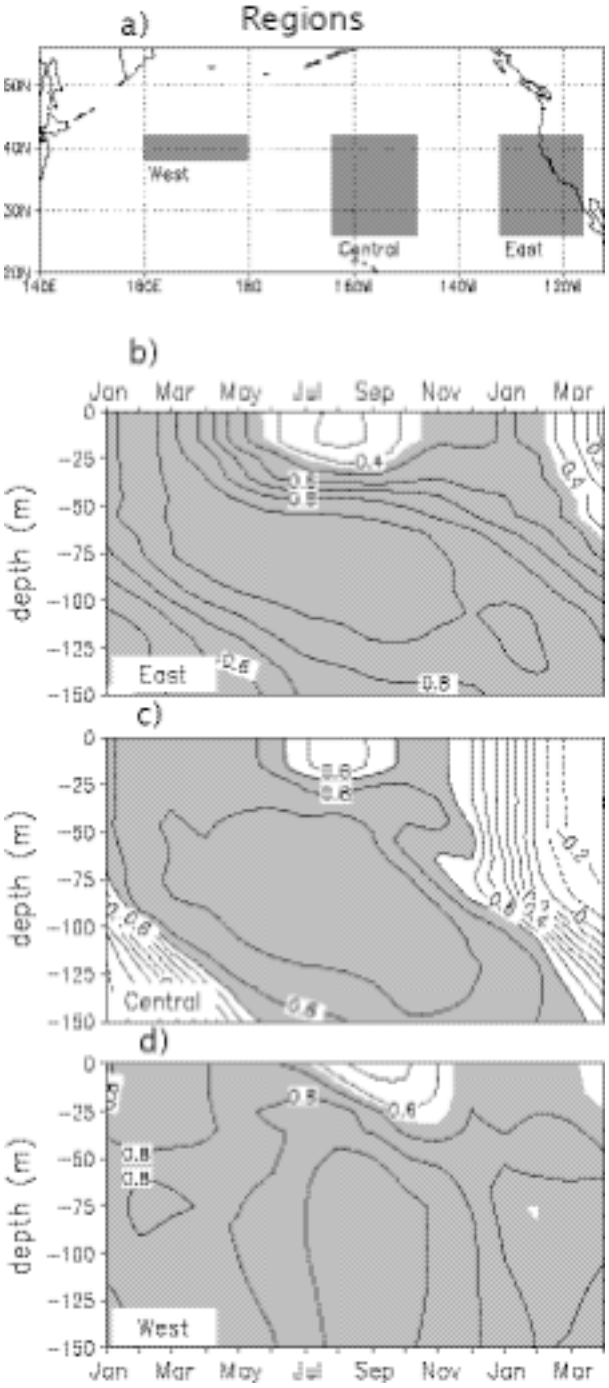

Figure 7. The reemergence mechanism as indicated by lead–lag regressions [°C (1°C)$^{-1}$] between temperature anomalies at 5 m in Apr–May, and temperature anomalies from the previous Jan through the following Apr in the (b) east, (c) central, and (d) west Pacific regions [shown in (a)]. The contour interval is 0.1 and values greater than (b) 0.55, (c) 0.7, and (d) 0.75 are shaded to highlight the reemergence mechanism. Computed using the NCEP ocean assimilation analyses [*Ji et al.*, 1995]. Adapted from *Alexander et al.* [1999].

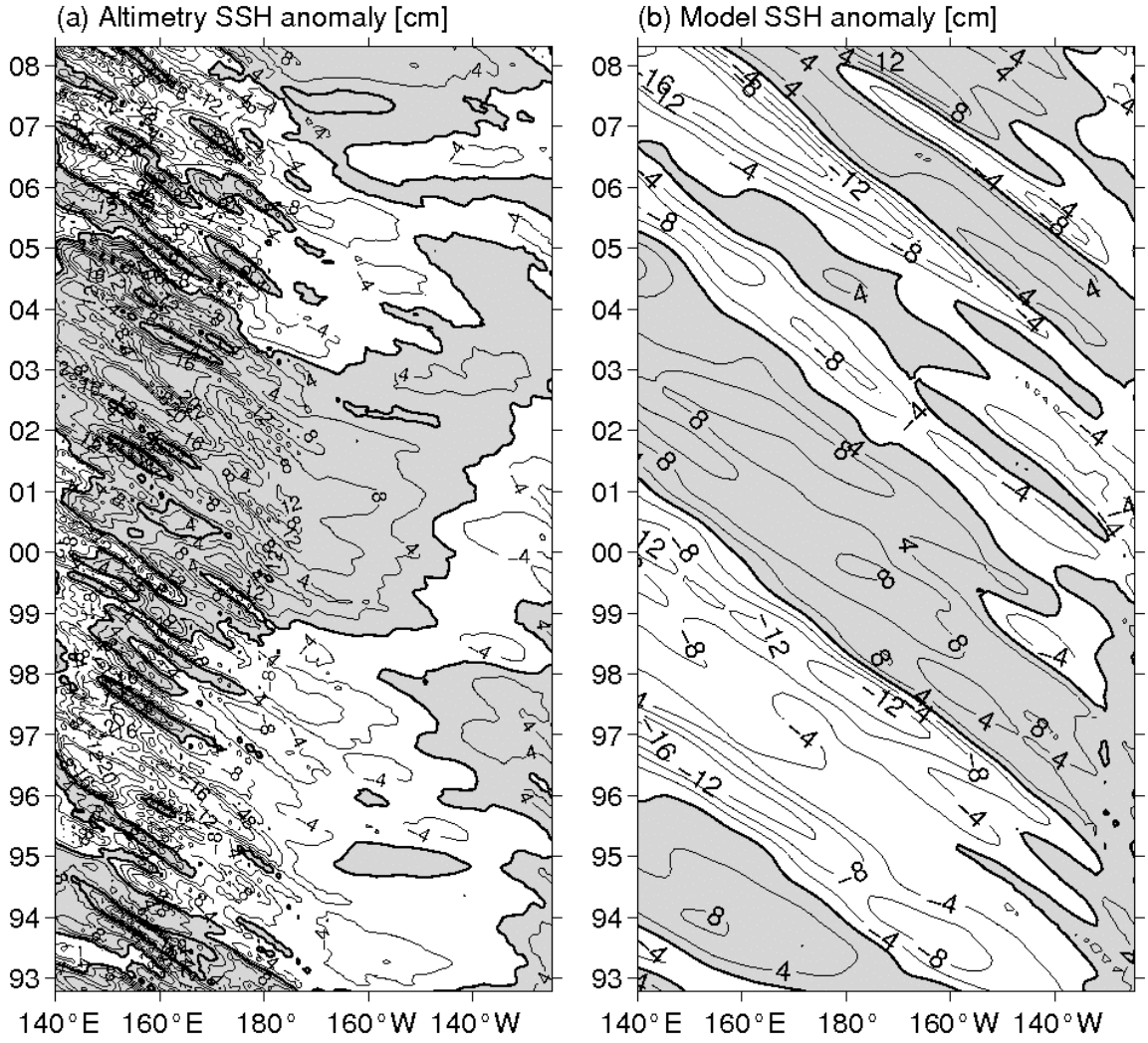

Figure 8. Sea surface height (SSH) anomalies along the zonal band of 32°–34°N from (a) the satellite altimeter data and (b) the wind-forced baroclinic Rossby wave model; see Eq. (5). Adapted from *Qiu et al.* [2007].

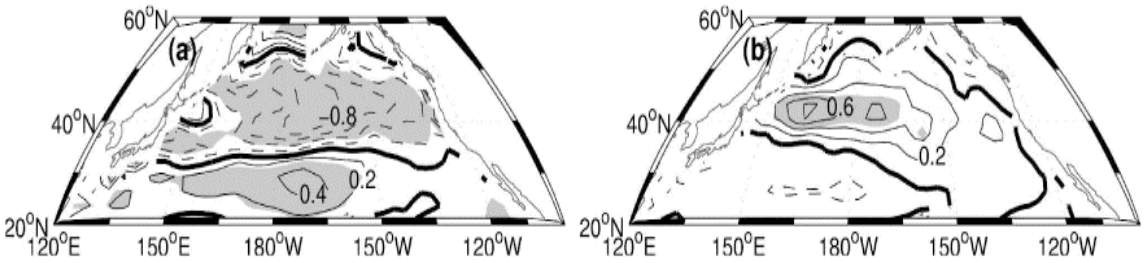

Figure 9. Atmospheric a) forcing and b) response to SST anomalies in the Kuroshio extension region. Regression of wind stress curl anomalies on the winter normalized SST anomalies in the KE region (35°–45°N, 140°E–180°). (a) Annual mean wind stress curl leading SST Index by 4 yr; both variables are smoothed with a 10-yr low-pass filter. (b) Annual mean wind stress curl lagging the SST index by 1 yr based on unfiltered data. The unfiltered regression pattern is further scaled by the ratio of the standard deviation of 10-yr low-pass-filtered SST index to that of unfiltered SST index. (Contour intervals are 0.2 × 10−8 N m−3. Negative values are dashed and shading indicates regressions significant at 99%. Results are from a long coupled NCAR GCM simulation. Adapted from *Kwon and Deser* [2007].

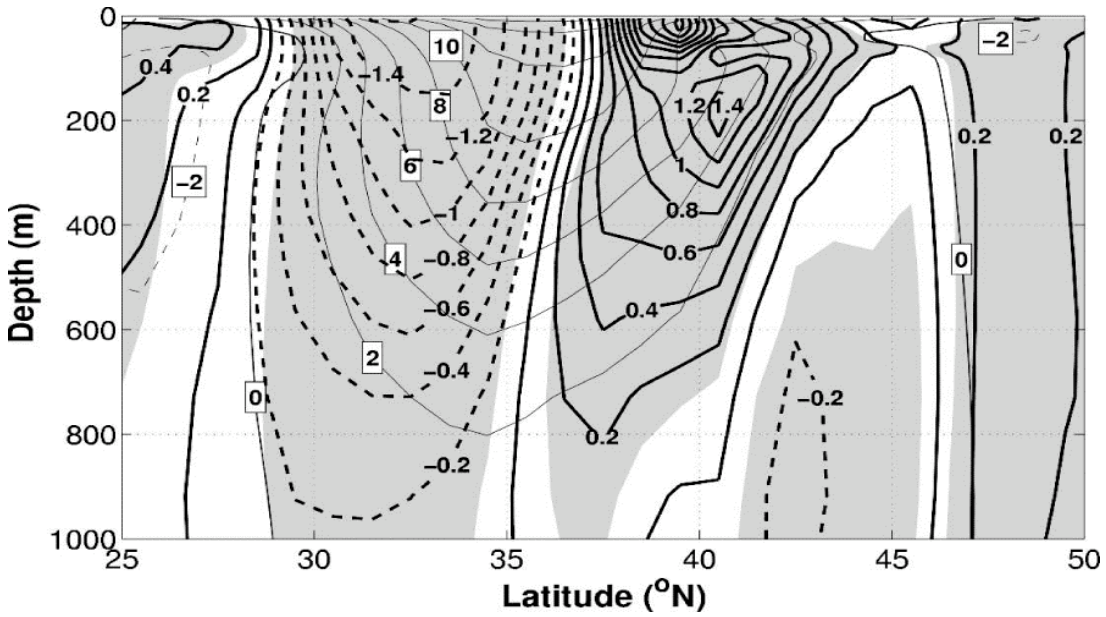

Figure 10. Relationship between temperature anomalies in the Kuroshio Extension and changes in the ocean gyres. Simultaneous regression of DJFM subsurface zonal current velocity along 150°E on the SST anomalies averaged over the KE region. Both variables have been low-pass filtered to retain periods longer than 10 yr. Contour interval is 0.2 cm s^{-1} °C^{-1}, and the shading indicates regressions significant at 99%. Solid (dashed) contours denote eastward (westward) velocity. Thin contours with boxed labels indicate the climatological winter (DJFM) mean zonal velocity fields. Contour interval for the mean zonal velocity is 2 cm s^{-1} Results are from a long coupled NCAR GCM simulation [*Kwon and Deser,* 2007]

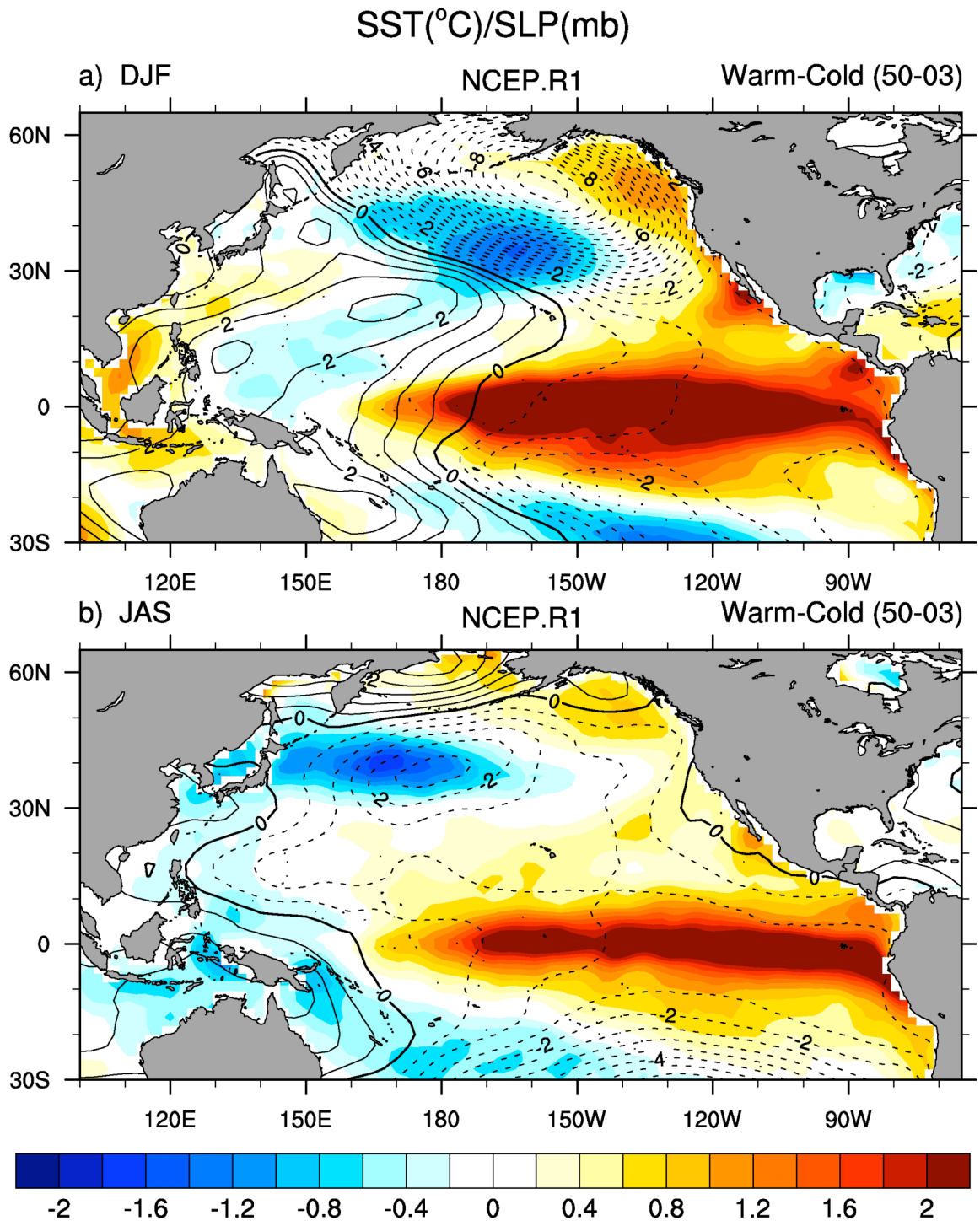

Plate 1. The ENSO signal including the atmospheric bridge as indicated by the composite of 10 El Niño minus 10 La Niña events for SLP (contours, interval 0.5 mb) and SST (shading, interval 0.2 °C) during (a) DJF when ENSO peaks and (b) the previous JAS. The fields are obtained from NCEP atmospheric reanalysis [*Kalnay et al.*, 1996; *Kistler et al.*, 2001].

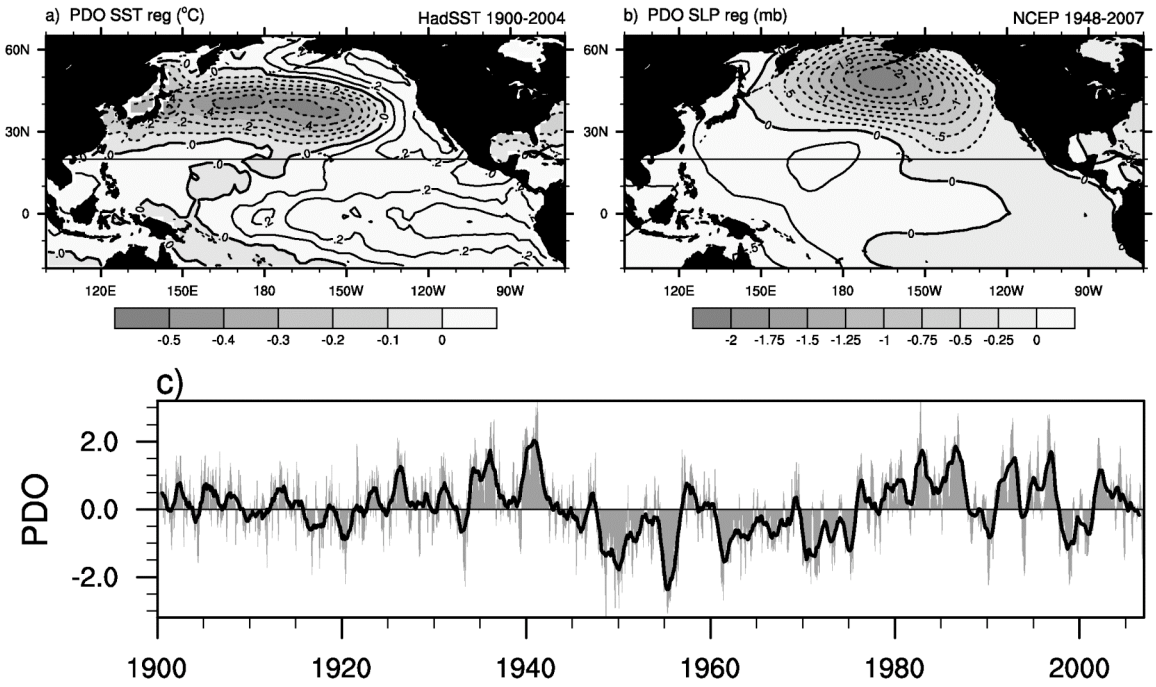

Figure 11. The Pacific Decadal Oscillation spatial and temporal structure: the leading pattern SST and SLP anomalies north of 20°N and normalized time series of monthly SST anomalies (PDO index, defined by Mantua et al. [1997]. Regressions of the PDO index on the (a) observed SST (ci 0.1 °C per 1σ PDO value) and (b) SLP (ci 0.25 mb per 1σ PDO value). The SSTs were obtained from the HadSST data set for the period 1900-2004, and the SLP values from NCEP Reanalysis for the years 1948-2007. (c) The monthly PDO index (gray shading) and 12-month running mean (black line) during 1900-2007, obtained from [http://jisao.washington.edu/pdo/PDO.latest].

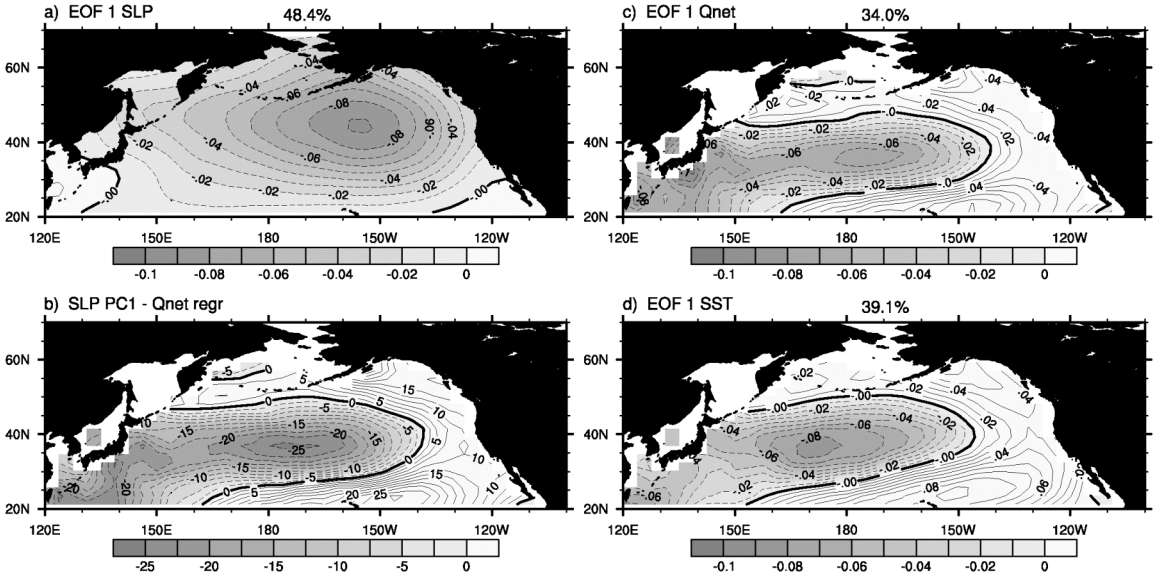

Figure 12. The SLP, flux and SST anomaly patterns associated with the Aleutian low during winter (DJF). (a) EOF 1 of SLP, regression values of the local (b) Qnet (contour interval 2.5 W m^{-2}) and (c) SST (CI is 0.05 deg C) anomalies on PC1 of SLP, (d) EOF 1 of SST. All fields are obtained from a 50-year simulation of the GFDL AGCM coupled to an ocean MLM over the ice-free ocean.

1454

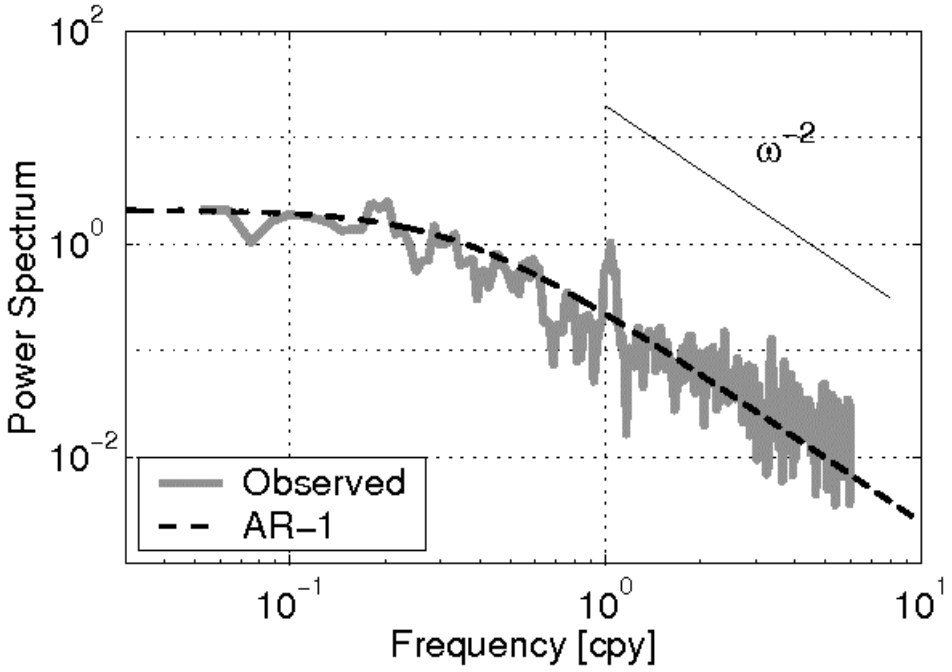

1455
1456
1457
1458 Figure 13. Power spectrum of the observed PDO index. Dashed indicates the best fit
1459 based on a first-order autoregressive model, thin solid line shows the theoretical slope for
1460 intermediate frequency portion of the spectrum from a stochastic model. Adapted from
1461 *Qiu et al.* [2007].
1462

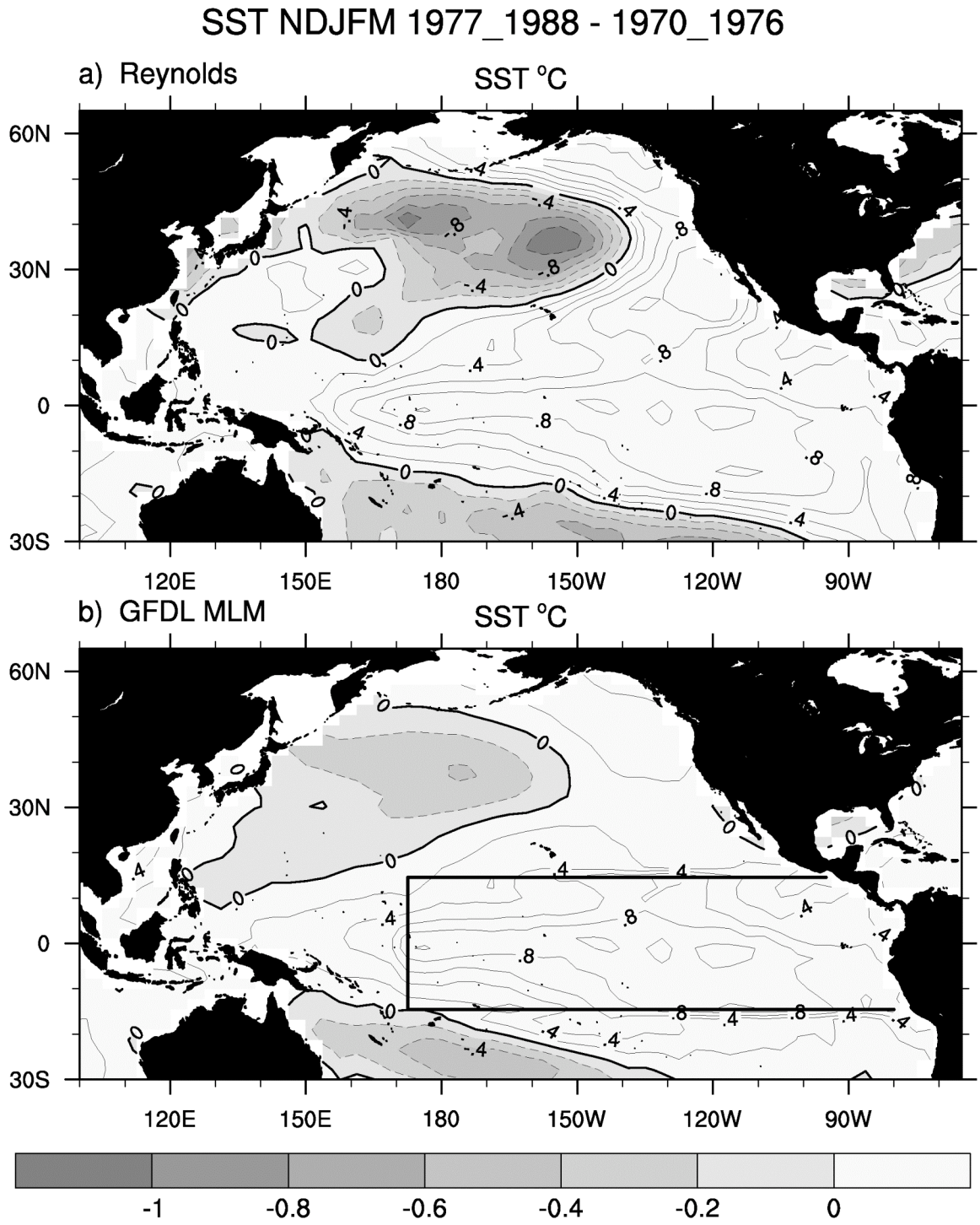

Figure 14. The 1977-1988 minus the 1970-1976 average SST during NDJFM from (a) observations and (b) an ensemble average of 16 model simulations. The observations and model integrations are described in *Smith et al.* [1996] and *Alexander et al.* [2002], respectively. The model consists of an AGCM coupled to an ocean mixed layer ocean model over the ice-free global oceans except in the central/eastern tropical Pacific (box) where observed SSTs are specified. Negative values are shaded and the CI is 0.2 °C.

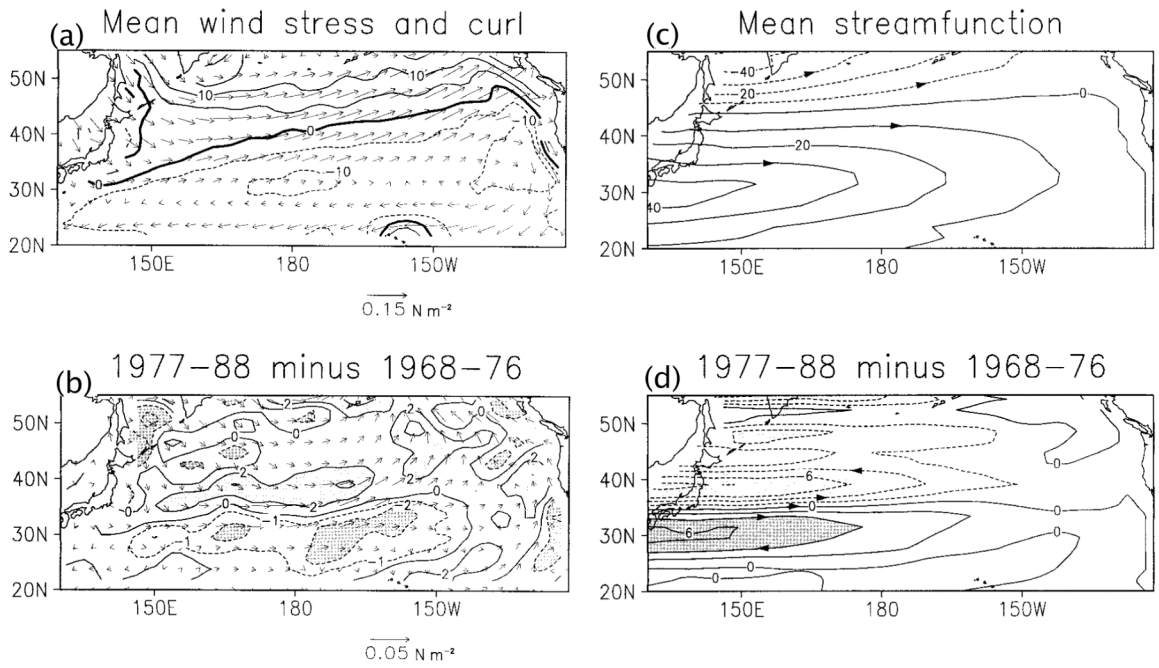

Figure 15. The annual a) long-term mean and b) 1977-88 minus 1986-76 wind stress (vectors) and its curl (contours) from the NCEP reanalysis. The ci is 5×10^{-8} N m^{-3} in a) and 2×10^{-8} N m^{-3} in b) where the $-1 \times 10-8$ N m-3 contour is also shown and values < $-2 \times 10-8$ N m^{-3} are shaded. The annual c) long-term mean and d) 1977-88 minus 1986-76 geostrophic transport streamfunction, given by the Sverdrup minus Ekman currents: the adjusted ocean circulation to wind curl forcing. The CI is 10 Sv in c) and 2 Sv in d), where values > 4 Sv are shaded. Adapted from Deser et al. [1999].

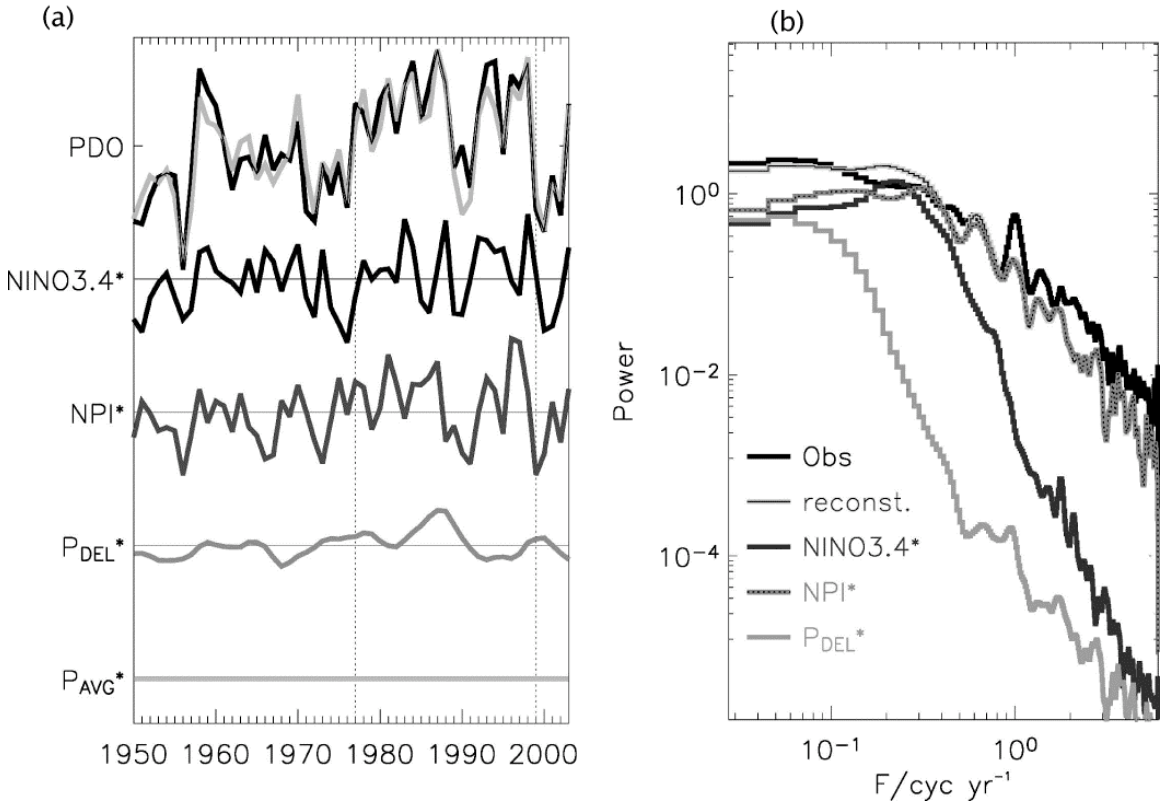

Figure 16. (a) The PDO time series and reconstruction (gray) based on contributions to the PDO from ENSO teleconnections (Niño-3.4*), stochastic fluctuations in the Aleutian low indicated by the North Pacific Index (NPI*), and the change in the ocean gyres given by the difference in the zonal average ocean pressure difference ($P_{DEL,}$ indicative of the slope of the thermocline and hence the strength/position of the ocean gyres) between 38° and 40°N in the KE region. The index for thermocline depth estimate from 35°-38°N in the KE region (P^*_{AVG}) does not explain a significant fraction of the SSTA variability of the PDO. Dotted vertical lines mark the winters of 1976/77 and 1998/99. (b) Power spectrum of the observed and reconstructed PDO, and contributions resulting from the NPI*, Niño34*, and P^*_{DEL}. Spectra have been smoothed by three successive applications of a five-point running mean. Note the dominance of the NPI* and ENSO* contributions to the PDO at internal annual time scales and the roughly equal contribution of the three factors at decadal time scales. From *Schenider and Cornulle* [2005].

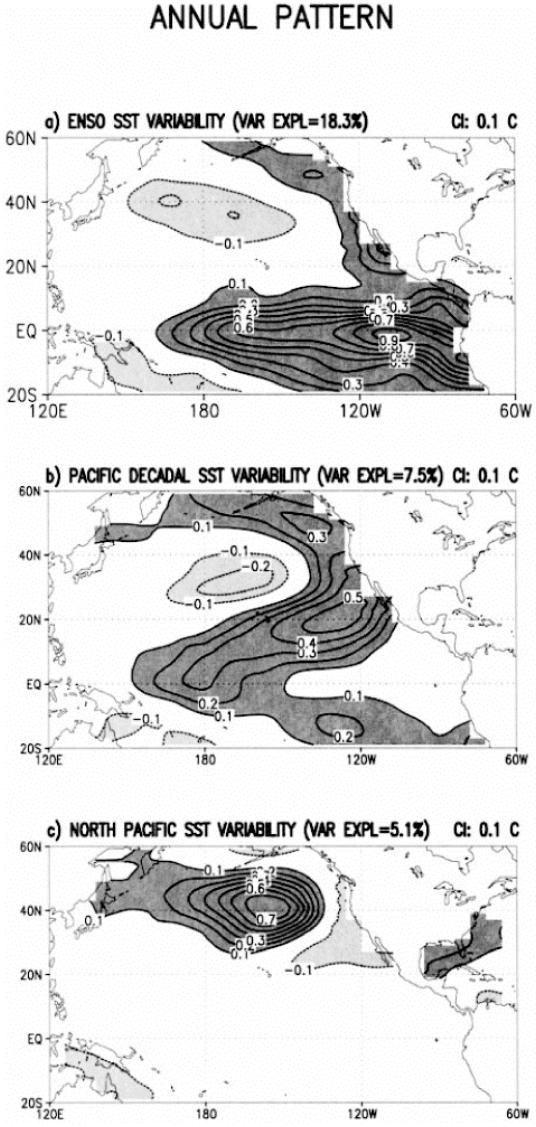

Figure 17. The spatial patterns for the three leading modes of Pacific SST variability during 1945–93 obtained from rotated principal component analysis: (a) ENSO, (b) Pacific Decadal Oscillation, and (c) North Pacific. Adapted from *Barlow et al.* [2001].